A new kannemeyeriiform dicynodont (Ufudocyclops mukanelai gen. et sp. nov.) from Subzone C of the Cynognathus Assemblage Zone (Triassic of South Africa) with implications for biostratigraphic correlation with other African Triassic faunas

Kammerer, Christian; Viglietti, Pia; Hancox, John; Butler, Richard; Choiniere, Jonah

DOI:
10.1080/02724634.2019.1596921

Document Version
Peer reviewed version

Citation for published version (Harvard):
Kammerer, C, Viglietti, P, Hancox, J, Butler, R & Choiniere, J 2019, 'A new kannemeyeriiform dicynodont (*Ufudocyclops mukanelai* gen. et sp. nov.) from Subzone C of the Cynognathus Assemblage Zone (Triassic of South Africa) with implications for biostratigraphic correlation with other African Triassic faunas', *Journal of Vertebrate Paleontology*, vol. 39, no. 2, e1596921. https://doi.org/10.1080/02724634.2019.1596921

A new kannemeyeriiform dicynodont (*Ufudocyclops mukanelai* gen. et sp. nov.) from Subzone C of the *Cynognathus* Assemblage Zone (Triassic of South Africa) with implications for biostratigraphic correlation with other African Triassic faunas

CHRISTIAN F. KAMMERER,[*,1,2] PIA A. VIGLIETTI,[2] P. JOHN HANCOX,[2] RICHARD J. BUTLER,[2,3] and JONAH N. CHOINIERE[2]

[1]North Carolina Museum of Natural Sciences, 11 W. Jones Street, Raleigh, U.S.A., christian.kammerer@naturalsciences.org;

[2]Evolutionary Studies Institute, University of the Witwatersrand, P.O. Wits 2050, Johannesburg, South Africa, pia.viglietti@gmail.com; jhancox@cciconline.com; Jonah.Choiniere@wits.ac.za;

[3]School of Geography, Earth and Environmental Sciences, University of Birmingham, Edgbaston, Birmingham, B15 2TT, United Kingdom, r.butler.1@bham.ac.uk

[*]Corresponding author.

ABSTRACT—A new taxon of kannemeyeriiform dicynodont, *Ufudocyclops mukanelai*, is described based on a well-preserved skull (BP/1/8208) from Subzone C of the *Cynognathus* Assemblage Zone, which are the youngest strata (probably Middle Triassic) of the Beaufort Group (uppermost Burgersdorp Formation) in South Africa. *Ufudocyclops* is diagnosed by its autapomorphic intertemporal morphology: the intertemporal bar in this taxon is 'X'-shaped—broad anteriorly and posteriorly but distinctly 'pinched' at mid-length, and bears a deep, triangular depression immediately behind the enormous pineal foramen. *Ufudocyclops* can also be diagnosed by the presence of a laterally-expanded jugal plate beneath the orbit and highly discrete, ovoid nasal bosses separated by a broad, unornamented median portion of the premaxilla and nasals. Two partial dicynodont skulls from this subzone (BP/1/5530 and BP/1/5531), previously identified as specimens of the otherwise Tanzanian taxon *Angonisaurus*, are also referable to *U. mukanelai*. Removal of these specimens from the hypodigm of *Angonisaurus* eliminates a crucial point of correlation between *Cynognathus* Subzone C and the Manda Beds of Tanzania, and suggests that Subzone C preserves a distinct, endemic fauna, not just a southern extension of the better-known Middle–Late Triassic tetrapod faunas from Tanzania and Zambia. Inclusion of *Ufudocyclops* in a phylogenetic analysis of anomodonts recovers it as an early stahleckeriid, the first record of this clade from the *Cynognathus* Assemblage Zone.

INTRODUCTION

The South African Beaufort Group preserves a ~30 Ma record of sedimentation extending from the middle Permian to the Middle Triassic (Smith et al., 2012). In addition to regional lithological subdivision of the Beaufort Group, this record is subdivided based on biostratigraphy into eight assemblage zones (AZs) characterized by and named after therapsid index taxa (Rubidge, 1995; Catuneanu et al., 2005). The youngest of these assemblage zones is the *Cynognathus* AZ, which is generally considered to range from the latest Early Triassic (Olenekian) to the early Middle Triassic (Anisian; Hancox, 2000; Abdala et al., 2005a; Neveling et al., 2005; although for uncertainty on this see Ottone et al., 2014). The *Cynognathus* AZ fauna is characterized by the initial diversification of eucynodonts, which would go on to become the most diverse Triassic therapsids and eventually give rise to mammals. Eucynodonts are the most species-rich component of this AZ and its index taxon is the large, predatory eucynodont *Cynognathus crateronotus*. Kannemeyeriiforms, which formed the major Triassic radiation of dicynodonts, also first appear in the African record in the *Cynognathus* AZ (Keyser and Cruickshank, 1979). Within the *Cynognathus* AZ, a highly characteristic fauna has long been recognized consisting of the eucynodonts *Cynognathus* and *Diademodon* and the kannemeyeriiform *Kannemeyeria* (Keyser and Smith, 1978; Keyser, 1979; Kitching, 1984; Rubidge, 1995). The shared presence of these three taxa in other basins has been used to correlate the *Cynognathus* AZ with other Gondwanan faunas, namely the Río Seco de la Quebrada Formation in Argentina (Bonaparte, 1966, 1969; Martinelli et al., 2009; note that the record of *Kannemeyeria* from this formation has been questioned, however; see Renaut and Hancox, 2001), Upper Omingonde Formation in Namibia (Keyser, 1973; Smith and Swart, 2002;

Abdala and Smith, 2009), Manda Beds in Tanzania (Cruickshank, 1965; Wynd et al., 2018), and lower Ntawere Formation in Zambia (Brink, 1963; Angielczyk et al., 2014; Peecook et al., 2018). Additional correlations with the upper Fremouw Formation in Antarctica have been made based on the presence of *Cynognathus* alone (Hammer, 1995).

Although the *Cynognathus-Diademodon-Kannemeyeria* assemblage was historically considered to range throughout *Cynognathus* AZ rocks in South Africa (Keyser and Smith, 1978), beginning in the 1990s, more detailed stratigraphic research began to question the uniformity of this assemblage zone (although *Cynognathus* does seem to be present throughout; see Abdala et al., 2005b). Hancox et al. (1995) proposed division of the *Cynognathus* AZ into three subzones (informally labeled A, B, and C) based on temnospondyl distribution and argued that most of the known *Cynognathus*, *Diademodon* and *Kannemeyeria* material from South Africa pertains to Subzone B. Subsequent research has supported the faunal distinction between these subzones. Notably, the members of the gomphodont eucynodont family Trirachodontidae are different in each subzone (Abdala et al., 2005a, 2006). Subzone A is the lowest of the three zones (usually considered Olenekian) and uniquely among the subzones yields specimens of the temnospondyl *Kestrosaurus* and the trirachodontid *Langbergia* (Shishkin et al., 1995; Abdala et al., 2006). Subzone B is usually considered early Anisian and is the most widely exposed and fossil-rich of the three subzones (Hancox et al., 1995; Abdala and Ribeiro, 2010). In addition to especially plentiful materials of *Cynognathus crateronotus*, *Diademodon tetragonus*, and *Kannemeyeria simocephalus*, this subzone is characterized by the presence of the temnospondyl *Xenotosuchus africanus* and the trirachodontids *Trirachodon berryi* and *T. kannemeyeri* (Damiani, 2008; Sidor and Hopson, 2018; note that the latter authors refer *T. kannemeyeri* to the genus *Cricodon*, albeit retaining it as a distinct species). The youngest of the three subzones,

Subzone C, is present only along a narrow series of hillside outcrops in the Eastern Cape. Hancox et al. (1995) considered this subzone likely to be late Anisian, and Shishkin et al. (1995) characterized it based on the presence of large capitosauroid amphibians, now assigned to the species *Paracyclotosaurus morganorum* (Damiani and Hancox, 2003). Additionally, Abdala et al. (2005a) described trirachodontid remains from Subzone C that they referred to *Cricodon metabolus*, a taxon originally described from the Manda Beds of Tanzania (Crompton, 1955).

While correlations between *Cynognathus* Subzone B and the aforementioned assortment of international Triassic assemblages have generally been retained to this day (Peecook et al., 2018; Wynd et al., 2018), correlates with subzones A and C have proven more problematic. Early Triassic tetrapod-bearing deposits are extremely rare globally and, of those, most correspond to the earlier *Lystrosaurus* AZ (e.g., the upper Guodikeng–lower Jiucaiyuan formations in China [Liu and Abdala, 2017], Panchet Formation in India [Ray, 2005], Upper Vetluga assemblage in Russia [Sennikov, 1996], and lower Fremouw Formation in Antarctica [Colbert, 1991]). Potentially coeval assemblages to Subzone A (the upper Jiucaiyuan Formation of China [Yang et al. 2000] and Yarenga assemblage in Russia [Sennikov and Golubev, 2006]) have comparatively little taxonomic overlap, making correlations more difficult, although the erythrosuchid genus *Garjainia* is shared between the South African and Russian assemblages (Sennikov, 1996; Gower et al., 2014).

Hancox and Rubidge (1996) referred a partial dicynodont skull (BP/1/5530, later described in greater detail by Hancox et al., 2013) from Subzone C to the genus *Angonisaurus*, a genus originally described on the basis of a single specimen (NHMUK PV R9732) from the middle-upper Lifua Member of the Manda Beds of Tanzania (Cox and Li, 1983; Smith et al., 2018). Based on this record and the presence of the trirachodontid *Cricodon*, Subzone C has

been correlated with the middle-upper Lifua Member of the Manda Beds and the upper Ntawere Formation of Zambia (Peecook et al., 2018).

Hancox et al. (2013) referred BP/1/5530 (and a second partial Subzone C skull, BP/1/5531) to *Angonisaurus* on the basis of the combination of a gently sloping intertemporal bar, postorbitals that do not extend the full length of the intertemporal bar to reach the squamosals, parietals widely exposed in dorsal view with a well-developed midline groove, and interparietal making a moderate contribution to the skull roof and meeting the parietals along an interdigitated suture. However, they hesitated to suggest conspecificity between the South African and Tanzanian specimens, leaving the former as *Angonisaurus* sp. and noting that new, more complete specimens would be required to provide a definitive taxonomic assessment of this material.

Recent excavations in *Cynognathus* Subzone C exposures by a team from the Evolutionary Studies Institute (University of the Witwatersrand, Johannesburg) and University of Birmingham (U.K.) have recovered a new, nearly-complete dicynodont skull closely matching the preserved morphology of the fragmentary specimens BP/1/5530 and BP/1/5531. Here, we describe this specimen, place it in phylogenetic context, comment on its relationships to *Angonisaurus*, and reevaluate the biostratigraphic implications of the Subzone C dicynodonts.

Institutional Abbreviations—**BP**, Evolutionary Studies Institute (ESI), University of the Witwatersrand, Johannesburg, South Africa; **GPIT**, Paläontologische Sammlung, Eberhard-Karls-Universität-Tübingen, Tübingen, Germany; **NHMUK**, the Natural History Museum, London, U.K.; **NMT**, National Museum of Tanzania, Dar es Salaam, Tanzania; **PIN**, Paleontological Institute of the Russian Academy of Sciences, Moscow, Russia; **PVL**, Instituto Miguel Lillo, Universidad Nacional de Tucumán, San Miguel de Tucumán, Argentina; **UFRGS**,

Universidade Federal Rio do Grande do Sul, Porto Alegre, Brazil; **UWBM**, University of Washington Burke Museum, Seattle, U.S.A.

GEOLOGICAL CONTEXT

The new dicynodont specimen (BP/1/8208) was discovered by Michael Day in 2014 and collected in 2017. It was found as an isolated, ventral-up skull within a fallen block of light greenish-grey (5GY 6/1), fine-grained sandstone of 1 m vertical thickness. The sandstone has a sharp lower contact that mostly comprises horizontally laminated sandstone and climbing ripples. The fossil was associated with an internal erosional boundary that contained rounded mud chips. The block comes from a unit that laterally becomes more channelized and thicker (~2.5 m) and contains trough cross-bedding. The unit has a gradational upper contact, grading first into ripple cross-laminated sandstone and then siltstone. Also, laterally the sandstone bed contains rooted horizons, which means it was periodically vegetated after deposition. Thus, the depositional context of the fossil points to burial during a flash flood event in either a small channel or a crevasse splay deposit. A large, as-yet-undescribed, partial cynodont skull was found in another fallen block, close to that containing the dicynodont and apparently from the same sedimentary unit. Stratigraphically, the new dicynodont lies approximately 65 m above the base of *Cynognathus* Subzone C (Fig. 1) and 45 m below the base of the Bamboesberg Member of the Molteno Formation (total thickness for Subzone C is 110 m; Hancox et al., 2013).

SYSTEMATIC PALEONTOLOGY

SYNAPSIDA Osborn, 1903

THERAPSIDA Broom, 1905

ANOMODONTIA Owen, 1860

DICYNODONTIA Owen, 1860

KANNEMEYERIIFORMES Maisch, 2001

STAHLECKERIIDAE Lehman, 1961

UFUDOCYCLOPS MUKANELAI gen. et sp. nov.

(Figs. 2–8)

Holotype—BP/1/8208 (Figs. 2–6), a well-preserved skull from the uppermost Burgersdorp Formation (*Cynognathus* Subzone C; ?Middle Triassic) on the farm Thala (Buffels Kloof), near Sterkstroom, Eastern Cape Province, South Africa (Fig. 1).

Referred Specimens—BP/1/5530 (Fig. 7), a partial skull roof (with left postorbital bar and fragment of zygoma) and isolated left caniniform process; BP/1/5531 (Fig. 8), various fragmentary portions of a skull (partial skull roof, caniniform processes, anterior palate, basicranium) and lower jaws. Assorted, largely unprepared postcranial elements (two partial humeri, a partial ulna, a partial radius, multiple vertebrae, and rib fragments) were also collected in association with BP/1/5331, but Hancox et al. (2013) considered them to be too large to pertain to the skull, a conclusion with which we agree. As no postcranial material is associated with the other definitive specimens of *Ufudocyclops mukanelai*, we cannot refer these elements to this taxon with confidence, and do not consider them further here. Preparation and study of these elements will be part of future research on the *Cynognathus* Subzone C fauna.

Diagnosis—Kannemeyeriiform dicynodont that can be distinguished by the following autapomorphies: paired, highly discrete, ovoid nasal bosses overhanging the external nares that are separated from each other by a broad segment of unornamented median premaxilla/nasal (shared with Permian cryptodonts, unique among kannemeyeriiforms); maxillary contribution to anteroventral corner of orbital margin; jugal with prominent, laterally-expanded suborbital plate limiting contribution of maxilla to zygomatic arch, and zygomatic arch generally with greater suborbital lateral expansion than other kannemeyeriiforms; intertemporal bar 'X'-shaped, anteriorly and posteriorly broad but with 'pinched' midpoint; parietals exposed in deep and broad but anteroposteriorly short depression posterior to pineal foramen.

Etymology—From the Xhosa *ufudo*, meaning tortoise (in reference to the toothless, tortoise-like beak), and the Ancient Greek *cyclops*, a one-eyed mythological giant (in reference to the enormous opening for the pineal eye on the dorsal midline of the skull). Species named in honor of Mr. Pepson Mukanela, in recognition of his many years working in the preparatory lab of the Evolutionary Studies Institute (and its predecessor, the Bernard Price Institute for Palaeontological Research) and in particular his skillful preparation of BP/1/8208.

DESCRIPTION

BP/1/8208

The skull is mostly complete, missing only the left temporal arch, the tips of the caniniform processes, and a small section of the snout that was sawed through when the specimen was collected. Accounting for this missing section, the complete skull is estimated to have been 29.0 cm long dorsally and 29.5 cm basally (Table 1). No lower jaw is preserved. Bone preservation on the skull is generally very good, with clear sutures visible on the face and palate

and surface ornamentation mostly intact, although there is some surficial wear dorsally on the snout and towards the back of the skull.

The anterior tip of the premaxilla was sawed off during excavation of the specimen so that the premaxilla is now separated into two portions: 1) a thin plate composed of the sawed-off anterior face of the premaxilla (Fig. 2A,B) and 2) the main portion of the premaxilla (including almost all of its palatal surface) still attached to the skull (Figs. 2C, 3, 4, 5). The anterior face of the premaxilla (Fig. 2A) is extremely rugose, with a series of pits and ridges running roughly dorsoventrally. This style of rugosity, which is present to varying degrees on much of the snout and palate, is usually considered to indicate extent of the keratinous beak in dicynodonts (Sullivan and Reisz, 2005; Kammerer et al., 2015). A weak but distinct midline ridge is present; it begins to taper out at the dorsal edge of the anterior premaxillary fragment and there is no sign of its continuation onto the main skull piece (Fig. 3). The internal bone structure is visible in cross-section where the premaxilla was cut through (Fig. 2B,C). The bone is highly trabecular, with a number of especially large trabeculae oriented dorsoventrally. No discrete, paired channels corresponding with vasculature are visible; the numerous pits on the premaxilla seem to be purely superficial, not foramina. The ascending process of the premaxilla forms the dorsal surface of the snout tip and extends posteriorly towards its contact with the mid-nasal suture. This contact is roughly midway between the orbits and nares, near the posterior margin of the nasal bosses (Fig. 3). The naso-premaxillary suture is relatively broad for a kannemeyeriiform; the posterior margin of the premaxilla is rounded rather than tapering to a sharp point as in many dicynodonts. Facially, the premaxilla forms the anterior margin of the naris and roughly the anterior half of its ventral margin (Fig. 4). The facial portion of the premaxilla is only weakly striated and lacks the distinct rugosity of the anterior and palatal portions. The suture between the

premaxilla and the maxilla is weakly angled posterodorsally; at the contact with the septomaxilla the suture then angles strongly anterodorsally. The facial surface of the premaxilla curves gently into the naris; there is not a discrete break in slope along the narial rim.

The palatal surface of the premaxilla is also highly rugose, but with finer pitting and without the small ridges present on the anterior surface (Fig. 5). The premaxilla forms a large plate making up the majority of the secondary palate in BP/1/8208. The palatal surface of the premaxilla is generally highly concave, but its central depression is broken up by the three prominent palatal ridges present in most dicynodonts: two paired anterior palatal ridges and one posterior median palatal ridge. The anterior palatal ridges likely would have extended almost to the tip of the snout, but their anterior terminus is cut off in this specimen. Deep grooves flank the anterior palatal ridges, with the deepest being the median groove between them. The anterior palatal ridges do not converge posteriorly or contact the posterior median palatal ridge, although the premaxillary surface is still weakly convex between these three ridges. The posterior median palatal ridge is taller than the anterior ones and becomes tallest at its posterior end near its contact with the vomer, with a rounded ventral expansion at the same height as the vomer. Laterally, the palatal surface of the premaxilla extends ventrally as thin laminae making up the dorsal edge of the medial surface of the caniniform process. This surface is more sparsely pitted than in the depressed portion of the premaxilla or on the palatal ridges.

The septomaxilla is restricted entirely within the naris (Fig. 4). Like the premaxillary contribution to the narial floor, it curves gently inwards from its border with the maxilla; there is not a sharp rim at the septomaxillary-maxillary suture. The lateral surface of the septomaxilla is generally concave, although there is a weak protuberance near the dorsal edge of the septomaxilla at mid-length, anterior to a small embayment in the septomaxillary margin.

Posteriorly, the septomaxilla is bordered by the maxilla and nasal; it does not contact the lacrimal.

The maxilla makes up the caniniform process, part of the lateral surface of the snout, and part of the anterior zygomatic arch (Fig. 4). The caniniform process does not bear tusks. As is typical for edentulous dicynodonts, the caniniform process is anteroposteriorly narrow with a notably concave posterior face (Fig. 5). The tips of the caniniform processes are broken off, but they were clearly angled anteroventrally. The lateral edge of the caniniform process extends posterodorsally towards the suborbital bar in the form of a ridge (the caniniform buttress), but the buttress is not massively robust as in *Rechnisaurus* or *Uralokannemeyeria*. The lateral and medial faces of the caniniform process are pitted and rugose, whereas the posterior face is smoother, becoming almost completely smooth where it forms the ventral surface of the zygoma. The facial surface of the maxilla, between the naris and orbit, is distinctly concave, but does not bear a discrete postnarial excavation. There is a dorsoventrally-oriented groove present at the center of the facial concavity on the right maxilla only. Dorsal to this concavity the maxilla curves outwards to contact the nasal and lacrimal; a weak ridge demarcates this suture. Near its contacts with the nasal and lacrimal dorsally (and jugal posteriorly) the maxillary surface is finely striated but not pitted. In lateral view, the maxilla is abruptly constricted posterior to the caniniform process, where it forms the anterior tip of the zygomatic arch. The maxilla is broadly exposed laterally and dorsally in the zygomatic arch anteriorly, and even contributes to a small portion of the anteroventral corner of the orbit (in most other kannemeyeriiforms, the ventral orbital rim is composed entirely of jugal). Slightly anterior to the orbital mid-length, however, the maxillary contribution to the zygoma is sharply restricted by a plate of the jugal extending

laterally. Posterior to this point the maxilla is reduced to a thin, tapering process on the ventral surface of the zygoma that terminates in a contact with the squamosal.

The nasal makes up part of the dorsal and lateral surfaces of the snout (Figs. 3, 4). Anterolaterally, the nasal bears a large, highly discrete, ovoid boss, overhanging the naris anteriorly (Fig. 5) and terminating near the anterior margin of the orbit. The boss on each nasal is separated from the other by a broad (3–7 cm), flat, unornamented portion of skull roof (made up of the premaxilla anteriorly and the nasals posteriorly). Although nasal bosses are present in most dicynodonts, in kannemeyeriiforms the bosses usually take the form of a rugose, expanded area extending across the dorsal surface of the snout. The bosses of *Ufudocyclops* are more similar in appearance to those of Permian cryptodonts, which also have highly discrete, rounded bosses separated from each other by a flat median span of snout. Somewhat similar bosses are seen in some kannemeyeriiforms (e.g., *Dolichuranus*), but in no other kannemeyeriiform are the bosses so discrete, with their edges so sharply demarcated from the surrounding snout. The surface of the nasal boss is heavily pitted, and with weak ridges similar to those on the anterior face of the premaxilla present at its anteromedial edge. Ventral to the boss, the nasal is exposed facially as a narrow strip of bone dorsal to the maxilla, which expands dorsoventrally into a short process near its posterior contact with the lacrimal. Dorsally, the nasal forms a nearly flat plate of bone making up a section of the midline of the skull roof. The bone surface of this part of the nasal is somewhat worn, and its suture with the frontal posteriorly cannot clearly be discerned. Based on the condition in BP/1/5530 (see below), we interpret *Ufudocyclops* as having a relatively short mid-nasal contribution to the skull roof.

The lacrimal is a small bone exposed at mid-height at the anterior margin of the orbit (Fig. 4). Facially, it has a short, roughly quadrangular exposure between the prefrontal, nasal,

and maxilla. Within the anterior orbital wall, the lacrimal extends ventrally; combined with the unusual maxillary contribution to the orbit it excludes the jugal from forming the orbital margin anteriorly. The lacrimal's suture with the prefrontal is notably ragged (with short, broad interdigitations); similar sutural morphology is present along the nasal-maxillary suture.

The jugal is very unusual in *Ufudocyclops*. Typically in dicynodonts, the zygomatic arch is composed mainly of the maxilla and squamosal in lateral view (King, 1988); the jugal is restricted to a thin exposure rimming the ventral edge of the orbit (although it makes a more substantial contribution to the zygoma ventrally). In *Ufudocyclops*, however, the jugal is excluded from this rim anteriorly by the lacrimal and maxilla, but posterior to that extends broadly laterally as a wide plate making up much of the suborbital zygoma (Figs. 3, 4). This expansion is associated with notable expansion of the suborbital zygoma in general, which flares out under the orbits (Fig. 2C) rather than curving gradually as in most kannemeyeriiforms. The jugal plate strongly constricts the posterior portion of the maxilla and limits its contribution to the zygoma. Posteriorly, this plate is overlapped by the broad footplate of the postorbital. The dorsal exposure of the jugal extends just posterior to the postorbital footplate, separating it from the squamosal and terminating with a very narrow contribution to the anteroventral margin of the temporal fenestra. Ventrally, the jugal is generally similar in morphology to those of other kannemeyeriiforms: a curved, flattened element rimming the subtemporal fenestra anterolaterally (Fig. 5). However, it also extends laterally (coming to a point where the zygoma flares), limiting the ventral maxillary contribution to the zygoma as well.

The squamosal makes up the majority of the zygomatic arch and is also a major contributor to the occiput (Figs. 3–6). Anteriorly, the squamosal contacts the maxilla roughly below the midpoint of the orbit (Fig. 4). From there it curves posterodorsally, forming a tall arc

subtemporally where it surrounds the attachment site for the M. adductor mandibulae externus lateralis. There is a distinct ridge ventrolaterally separating the lateral face of the squamosal from the ventral portion showing muscle attachment. Medial to this arc, another ramus of the squamosal extends to form the posterior edge of the temporal fenestra. Posteriorly, the squamosal makes up roughly half of each side of the occipital plate (Fig. 6). It has a raised edge at its lateral margin (as in *Angonisaurus*), then bears a tall concavity on its occipital face. Although occipital sutures are poorly preserved in this specimen, the squamosal appears to contact the tabular and a complex of apparently fused bones (normally it would contact the lateral edges of the supraoccipital and opisthotic when these bones are distinct) at its medial edge, and forms the lateral margin of the post-temporal fenestra.

The prefrontal makes up the anterodorsal corner of the orbital margin, where it forms a rugose, expanded boss (Figs. 3, 4). This boss does not extend onto the lacrimal ventrally and only weakly onto the frontal posteriorly; it is mostly a prefrontal feature and not a continuous circumorbital rim (though a comparable boss is also present at the posterodorsal corner of the orbit on the postorbital bar). Anterior to this boss, the prefrontal has a very short, depressed contribution to the lateral snout surface before contacting the nasal boss. It does not contact the maxilla. Dorsally, the prefrontal extends posteromedially as a broadly triangular process impinging on the otherwise naso-frontal interorbital region.

The exact dimensions of the frontal are uncertain in BP/1/8208, because as discussed above there is not a clear suture with the nasal and the bone surface in this region is damaged. The frontal in kannemeyeriiforms generally has an anterior process (King, 1988); we interpret the same as being present in BPI/1/8208, and reconstruct its extent in Figure 3 based on the somewhat indistinct lines we suspect correspond to the naso-frontal sutures (as well as

comparisons with BP/1/5530). A clear midline suture is present in the interorbital region: it is essentially straight anteriorly and ragged posteriorly. The greatest interdigitation along this suture is present on a midline eminence anterior to the pineal foramen. Such an eminence, with dense interdigitation of the midline suture, is present in many kannemeyeriiforms (Kammerer, pers. obs.). A similar structure is also present in gorgonopsians (Kammerer, 2016) and possibly represents structural response to similar strains on the skull in these taxa. Other than at this eminence, the surface of the frontal is flat to slightly concave. A few very small pits are present on the frontal surface, but nothing like the dense rugosity and pitting suggestive of keratinous covering on the snout and palate. Posterolaterally, the frontal has an irregular suture with the postorbital, originating at the posterodorsal corner of the orbit and continuing along the dorsal margin of the temporal fenestra. Posteriorly, the frontal extends into the intertemporal region as a tapering process extending between the temporal fenestra and pineal foramen. It terminates near the posterior edge of the pineal foramen at a contact with the parietal. This process is quite broad anteriorly and excludes the postorbital from making much of a dorsal contribution to the intertemporal bar; the latter bone is exposed dorsally as only a thin strip at the edge of the temporal fenestra. Posteromedially, the frontal surface slopes ventrally to form the anterior wall of the depression housing the pineal foramen. The prepariental appears to have been absent (as described by Hancox et al. [2013] for BP/1/5530), as is the postfrontal (as is typical of kannemeyeriiforms; Angielczyk et al., 2018).

The postorbital consists of two rami: 1) the postorbital bar which extends ventrally and makes up the anterior margin of the temporal fenestra and posterior margin of the orbit and 2) a posteriorly-directed process forming part of the medial wall of the temporal fenestra (Figs. 3, 4). The ventral base of the postorbital bar is a broad footplate lying on top of the jugal, which then

constricts dorsally between the orbit and temporal fenestra. The postorbital bar is weakly twisted at mid-height and bears a low ridge at its anterior edge around this point. This ridge expands dorsally and posteriorly to become a rugose boss, comparable to that on the prefrontal. The skull roof portion of the postorbital is initially exposed as a ragged strip of bone (because of its irregular suture with the frontal) at the anterior edge of the temporal fenestra (medial to the postorbital bar). This portion is weakly concave but does not have an extensive, discrete shelf dorsally serving as the attachment site for jaw musculature as in many other dicynodonts. There is a ridge separating the dorsal exposure of the postorbital from the portion making up the anteromedial wall of the temporal fenestra; this break in slope probably corresponds to the zone of attachment of the M. adductor mandibulae externus medialis (Angielczyk et al., 2018). The postorbital only makes up the anterior half of the medial wall of the temporal fenestra; posteriorly this wall is made up of a lateral exposure of the parietal. There is a diagonal suture running anterodorsally to posteroventrally between these two bones (Fig. 4).

The intertemporal bar in *Ufudocyclops* is unique among kannemeyeriiforms in having a distinct ‘X’-shape, in which it is broad anteriorly and posteriorly and ‘pinched’ in the middle (Fig. 3). The anterior two legs of the ‘X’ are made up of the frontals and postorbitals, whereas the posterior legs are mostly made up of the postparietal. The center of the ‘X’ is made up of a small dorsal exposure of the parietals. The parietals are exposed in a depression on the skull roof posterior to the pineal foramen; in BP/1/8208 each parietal also bears a slightly deeper depression at the center. The parietals are divided posteriorly by a tapering anterior process of the postparietal, and they continue as attenuate posterior processes flanking it. Laterally, the parietals form the posterior portion of the medial wall of the temporal fenestra, as described above.

The postparietal is well-exposed dorsally in the intertemporal bar (Fig. 3). In addition to making up most of the posterior half of the intertemporal 'X', it forms the posterodorsal edge of the temporal fenestra, overhanging the strongly concave parietal wall of the temporal fenestra. Posteriorly, the postparietal curves downwards onto the occiput, forming a broad plate at the dorsal occipital margin (Fig. 6). Its occipital face is depressed relative to the rest of the occiput, although it has a very weak nuchal crest medially with concavities to either side.

The tabular is poorly preserved in BP/1/8208; it is missing on the left side and on the right side appears to be restricted to the ventral surface of the laminar posterior edge of the temporal fenestra (Fig. 6). The supraoccipital is a median occipital bone forming the dorsal margin of the foramen magnum. Its dorsal margin is impinged on by the broadly rounded occipital portion of the postparietal, giving the supraoccipital the appearance of a pair of 'wings'. Distinct sutures between the supraoccipital, exoccipitals, opisthotic, and basioccipital are not visible, and it is likely that these elements are fused in *Ufudocyclops*, as is the case in many dicynodont taxa (Kammerer et al., 2015). A plate-like element forming part of the medial wall of the temporal fenestra, exposed ventral to the parietal and postorbital in lateral view (Fig. 4), is tentatively identified as prootic based on position, but it is likely that this element is also fused with the aforementioned occipital bones to form a single periotic element. The lateral edges of the foramen magnum bear thick rims that increase in robustness ventrally, terminating in knob-like processes (points of articulation with the proatlases) separated from the underlying occipital condyle by a horizontal depression (Fig. 6). Lateral to these processes are a second pair of knob-like processes of roughly equivalent size. The post-temporal fenestra is oval in shape with its long axis oriented dorsolateral-to-ventromedially. It lies between the squamosal laterally and presumably fused portions of the supraoccipital and opisthotic medially. Ventral to the post-

temporal fenestra, a tall, robust paroccipital process is present, coming to a sharp point posteroventrally. The occipital condyle is a large, tripartite structure; although sutures are not visible, the three lobes of the condyle were presumably made up of the two exoccipitals and a median basioccipital as in all other dicynodonts (King, 1988). A weak depression is present centrally on the occipital condyle between the presumed exoccipital and basioccipital portions. To either side lateral to the occipital condyle is a large, circular jugular foramen.

The vomer is mainly exposed as a narrow, rod-like median element within the interpterygoid vacuity (Fig. 5). Posteriorly, it expands into paired laminae that overlap the pterygoids and form the posterior wall of the interpterygoid vacuity.

The palatine is a small bone in *Ufudocyclops*. Anteriorly the palatine is made up of a palatine pad forming the posterior edge of the secondary palate (Fig. 5). This pad is heavily pitted and rugose and likely bore a cornified surface. Posterior to this pad, the palatine forms a thin lamina making up the lateral wall of the interpterygoid vacuity. The lateral palatal foramen is present as an elongate oval opening between the palatine and anterior ramus of the pterygoid, located posterodorsal to the palatine pad. No ectopterygoid is visible in this specimen. This element is missing in some other kannemeyeriiforms as well (e.g., Angielczyk et al., 2018).

The pterygoids form the characteristic ‘X’-shaped complex made up of paired anterior and posterior rami present in all dicynodonts (Fig. 5). The anterior rami are elongate, robust structures, and bear distinct ventral eminences (the anterior pterygoid keels) near their anterior tips (Fig. 4). The median pterygoid plate is damaged but appears to have been weakly concave. The posterior (quadrate) pterygoid rami are unfortunately also damaged; only their bases are preserved, but they indicate a strong degree of curvature laterally.

There is a sharp break in slope between the posterior edge of the pterygoids and the anterior edge of the parabasisphenoid. The median surface of the parabasisphenoid forms a narrow anteroposteriorly elongate depression extending between the basal tubera; no intertuberal ridge is present. The basal tubera are anteroposteriorly longer than wide and are nearly straight along their medial edges (Fig. 5). A distinct suture on the basal tuber between the parabasisphenoid and basioccipital is not visible, and it is possible that these too are fused in this specimen. Ventrolateral to the paroccipital process on the right side of the skull is a portion of the quadrate. Unfortunately, not much can be said about the morphology of this element, as it is incomplete and poorly preserved.

BP/1/5530

This specimen and BP/1/5531 were described by Hancox et al. (2013) as *Angonisaurus* sp. As both of these specimens were described in detail by Hancox et al. (2013), the following redescriptions will focus on areas of anatomy not preserved in or differing from BP/1/8208. BP/1/5530 consists of an isolated partial left caniniform process and a partial skull made up of the median dorsal edge of the occipital plate, the intertemporal bar, partial interorbital region, left postorbital bar, and a fragment of zygomatic arch (Fig. 7). The proportions of this specimen indicate that it was a somewhat larger animal than BP/1/8208: the distance from the anterior edge of the pineal foramen to the posterior edge of the intertemporal bar is 10.0 cm in BP/1/8208 and 11.0 cm in BP/1/5530 (this region is incomplete in BP/1/5531, but is estimated to have been ~9.5 cm in length). The margin of the left orbit is preserved in BP/1/5530 and shows that this individual also had expanded orbital rims on the prefrontal and postorbital. The bone surface texture of the interorbital region is better preserved in BP/1/5530 than in BP/1/8208 and shows a distinctly radiating ‘starburst’ pattern indicating a zone of bone growth that here we interpret as

corresponding to the frontal. At the anterior edge of the specimen, on the more complete left side, there is a small portion of skull roof with a differing, anteroposteriorly striated rather than radiating surface texture. This region is offset from the inferred frontal region by a narrow groove. We suggest that this break in ornamentation represents the border between the frontal and the nasal and prefrontal, with the groove representing the naso-frontal suture. This would indicate that the frontal makes up most of the interorbital skull roof in *Ufudocyclops*, and extends somewhat anterior to the orbit in the form of a median process (as shown in the interpretation of BP/1/8208 in Figure 3).

The postorbital in BP/1/5530 (Fig. 7C) has a greater dorsal contribution to the anterolateral rim of the temporal fenestra than in BP/1/8208, although this may be due to dorsoventral compression of this specimen (which clearly was present based on the distorted shape of the postorbital bar; Fig. 8B). Dorsoventral compression would also explain the more dorsally-directed postorbital-parietal medial wall of the temporal fenestra, which is nearly vertical in BP/1/8208. Legitimate differences in morphology seem to exist between these specimens in the intertemporal bar. Although both specimens show the autapomorphic 'X'-shape with an anterior depression behind the pineal foramen and posterior expansion of the postparietal, in BP/1/5530 the center of the 'X' is more pinched than in BP/1/8208. The parietal depression (Fig. 7A, C) is also narrower and deeper in BP/1/5530 than in BP/1/8208, and there does not appear to be a median ridge along the mid-parietal suture (although this may be damaged or overprepared in this specimen). We interpret the postparietal as having a substantial contribution to the intertemporal bar in BP/1/5530, contra Hancox et al. (2013:Fig. 2), who reconstructed this region as being made up mostly of parietal, based on re-examination of this specimen and direct comparison with BP/1/8208.

Unfortunately, the ventral surface of BP/1/5530 is poorly preserved and does not show distinct sutures. Well-developed but small fossae are present laterally on the underside of the intertemporal bar, extending across the postorbital and parietal. The fragment of zygoma preserved as part of this specimen includes the posterior portion of the jugal, which shows a broad, flattened plate dorsally, as in BP/1/8208. The isolated caniniform also accords with the condition in BP/1/8208, but is preserved all the way to the tip, showing that it came to a blunt tip (Hancox et al., 2013:Fig. 2).

BP/1/5531

This specimen consists of a large portion of skull made up of the snout tip (preserving the anterior palate and caniniform processes but not any of the dorsal surface) articulated with the anterior lower jaws (Fig. 8A–E), another skull portion made up of the intertemporal bar, occiput, and basicranium (Fig. 8F), and a series of small fragments. Although the dorsal portion of the intertemporal bar on this specimen is damaged, it can also be referred to *Ufudocyclops mukanelai* based on the presence of a depressed parietal exposure behind the pineal foramen and a 'pinched' midpoint of the intertemporal bar (Hancox et al. 2013:Fig. 3B). It also accords with BP/1/8208 and BP/1/5530 in other preserved morphology: the caniniform processes are edentulous, have the same shape as BP/1/5530 (Fig. 8C–E), and flare laterally like BP/1/8208 (compare Fig. 2C and Fig. 8C), the anterior palate is very heavily pitted (with ridges and rugosities preserved even better than in BP/1/8208), the pineal foramen is proportionally huge, the postparietal bears a weak nuchal crest and strongly constricts the supraoccipital above the foramen magnum, and the basal tubera are longer than wide. Although generally similar to the isolated caniniform process in BP/1/5530, the processes in BP/1/5531 are not compressed, and

show that their ventral margin curves inwards anteriorly before curving out towards the contact with the premaxilla.

Although fragmentary, BP/1/5531 does preserve important points of morphology not present in the other specimens of *U. mukanelai*, notably the lower jaw (not present at all in either other specimen) and quadrate-quadratojugal complex (present only as a badly damaged fragment on one side in BP/1/8208) (see Hancox et al. 2013:Figs. 3, 4E–H). The preserved portion of the lower jaw consists of the anterior portion of the mandibular rami, missing the tip and broken off at the level of the mandibular fenestrae (although a fragment of the articular region is also preserved in another piece of the skull; see below). Preserved elements include the dentary, splenial, and angular. The anterior face of the mandibular symphysis is highly rugose and made up mostly of the fused dentary, but with a sizable, triangular ventral contribution from the fused splenial. The angular does not contribute to the symphysis as preserved, but as the ventral edge of the jaw is eroded off this may be taphonomic: extension of the angular into the symphysis is typically present in kannemeyeriiforms (Kammerer, 2018). Although not as sharp as in *Stahleckeria*, there does appear to be a break in slope between the anterior surface of the symphysis and the lateral face of the dentary; it does not evenly curve around. Dorsally, the left dentary table is exposed immediately posterior to the symphysis. It is broadest anteriorly and tapers posteriorly; dorsally it narrows to a thin ridge. Lateral to the table is an elongate groove (the dentary sulcus) with a pitted texture. The lateral dentary shelf is low and narrow and extends slightly anterior to the mandibular fenestra. Only the anterior tip of the mandibular fenestra is preserved; it appears to be dorsoventrally narrow but this may be due to crushing. The splenial makes a tall contribution to the posterior face of the symphysis. A median foramen is present at

the posterior contact between the dentary and splenial. A pair of depressions is present near the ventral edge of the splenial on its posterior face; these are typically present in dicynodonts.

A large portion of the quadrate-quadratojugal complex is preserved on the left side of the skull (Hancox et al. 2013:Fig. 3). As is typical for dicynodonts, these bones are fused into a single unit, but a large, circular quadrate foramen is present between them. The complex flares outwards laterally, as is also the case in various stahleckeriids (Angielczyk et al. 2018). The quadrate condyles are preserved in articulation with the articular bone of the lower jaw. They are large and rounded with a well-developed median sulcus to accommodate the dorsal ridge of the articular. A retroarticular process is present on the ventral surface of the articular and weakly curves medially, terminating in a blunt tip.

PHYLOGENETIC ANALYSIS

Ufudocyclops mukanelai was included in a phylogenetic analysis based on the most recent analyses of anomodont therapsids (those of Angielczyk and Kammerer, 2017; Kammerer, 2018; and Angielczyk et al., 2018). These analyses were all based on the same underlying data set and differ only in minor details of taxon inclusion and character coding; the information from all three has been combined in the current analysis (see Supplementary Data 1 and 2). The data set consists of 105 OTUs (mostly at the species level; genus level utilized only for genera whose alpha taxonomy still requires revision, such as *Shansiodon* and *Sinokannemeyeria*) and 197 characters (174 discrete state and 23 continuous). Seven discrete state characters were treated as ordered (characters 58, 61, 79, 140, 150, 151, 166). Continuous characters were treated as additive based on the methodology of Goloboff *et al*. (2006). Continuous character codings were

based on within-OTU means for taxa represented by multiple specimens. The character set is the same as that of Kammerer (2018), with revised codings for *Compsodon* and *Sangusaurus* based on the data sets of Angielczyk and Kammerer (2017) and Angielczyk et al. (2018), respectively. Discrete-state character codings for *Ufudocyclops* were based on BP/1/5530, BP/1/5531, and BP/1/8208; continuous characters could only be coded for BP/1/8208.

The data set was analyzed using TNT v1.1 (Goloboff et al., 2008) using New Technology methods (tree drifting, parsimony ratchet, and tree fusing) on a driven search (initial search level=65, checked every three hits) with 500 initial addition sequence replicates required to find shortest tree length 20 times. Analysis of the complete dataset yielded three most parsimonious trees of length 1157.559 (consistency index=0.238, retention index=0.718). The three trees differed only in the topology within the stahleckeriid subclade Placeriinae, with the strict consensus (Fig. 9) showing a polytomy between *Moghreberia*, *Pentasaurus*, *Placerias*, and *Zambiasaurus* (as in Kammerer, 2018). Reanalysis of the dataset following removal of the extremely incomplete (only codable for 22/197 characters) taxon *Pentasaurus goggai* yielded a single most parsimonious tree of length 1155.559 (consistency index=0.239, retention index=0.717). This tree differed from the one including *Pentasaurus* only in showing greater resolution within Placeriinae (*Zambiasaurus* (*Moghreberia+Placerias*)), otherwise the two were identical. Resampling analysis was run on this jackknifed dataset, using symmetric resampling with 10000 replicates.

Ufudocyclops mukanelai was recovered as a stahleckeriine stahleckeriid, forming the sister-taxon of *Stahleckeria potens*. The topology within Stahleckeriinae differs from that of both Angielczyk et al. (2018) and Kammerer (2018), being ((*Ufudocyclops mukanelai* + *Stahleckeria potens*), (*Sangusaurus parringtonii* (*Eubrachiosaurus browni* (*Ischigualastia jenseni* +

Jachaleria)))). In Angielczyk et al.'s (2018) analysis, *Sangusaurus* was recovered as the sister-taxon of *Stahleckeria*, and in Kammerer's (2018), *Sangusaurus* and *Stahleckeria* were part of an unresolved polytomy at the base of Stahleckeriinae. Topology for the rest of Kannemeyeriiformes is mostly the same between the current analysis and that of Angielczyk et al. (2018) and Kammerer (2018), although the current analysis finds *Tetragonias* and *Vinceria* to be successive outgroups as part of a paraphyletic "Shansiodontidae", rather than sister-groups to each other. Although broader anomodont phylogeny for the most part is consistent between all three analyses, continued instability is present among non-kannemeyeriiform dicynodontoid taxa. In the current analysis an expansive Dicynodontidae containing *Daptocephalus*, *Delectosaurus*, *Dicynodon*, *Dinanomodon*, *Peramodon*, *Turfanodon*, and *Vivaxosaurus* forms the sister-taxon of *Lystrosaurus*, and a clade made up of *Gordonia* and *Jimusaria* forms the sister-taxon of Kannemeyeriiformes. *Euptychognathus*, *Syops*, and a clade made up of *Basilodon* and *Sintocephalus* form successive sister-taxa to the clade containing ((Dicynodontidae+Lystrosauridae) Kannemeyeriiformes). As discussed by Angielczyk and Kammerer (2017), basal Dicynodontoidea represents the most problematic part of dicynodont phylogeny at present, and much more work is required before a robustly-supported phylogenetic hypothesis will be available for this part of the tree.

The position of *Ufudocyclops* as sister-taxon of *Stahleckeria* is supported by two characters (Continuous Character 8, width of median pterygoid plate, and Discrete State Character 89, anterior pterygoid keel restricted to tip). However, this taxon differs from other stahleckeriines in its extremely broad frontal contribution to the orbital margin, similar to earlier-diverging kannemeyeriiforms. It requires only 1.153 steps to pull *Ufudocyclops* outside of the clade containing the other stahleckeriines, and given the low stratigraphic position of

Ufudocyclops it is not unreasonable to suspect that it actually represents the basalmost member of this clade. Additional research on early stahleckeriid morphology is required; unfortunately, reconstruction of the ancestral condition for Stahleckeriidae is complicated by the fact that the first-appearing placeriine (*Zambiasaurus*) is known only from extremely fragmentary, mostly juvenile material (Angielczyk et al., 2014).

DISCUSSION

Distinction of *Ufudocyclops* from *Angonisaurus*

Hancox et al. (2013) referred BP/1/5530 and BP/1/5531 to the genus *Angonisaurus*, and this referral has become a pivotal data point in correlating *Cynognathus* Subzone C with the Manda Beds in Tanzania (and potentially, by extension, the upper Fremouw Formation of Antarctica; see Sidor et al., 2014). Originally, *Angonisaurus* was known from a single specimen (NHMUK PV R9732, the holotype of *A. cruickshanki*, consisting of a complete but somewhat poorly preserved skull [Fig. 10B, D], lower jaw, partial left scapulocoracoid, partial left humerus, complete left pelvis, and assorted vertebrae and ribs) from the middle-upper Lifua Member of the Manda Beds in Tanzania (Cox and Li, 1983; Angielczyk et al., 2014). Despite extensive subsequent field work in the Manda Beds (Sidor and Nesbitt, 2018), only a single specimen referable to *Angonisaurus cruickshanki* has been found there since: NMT RB155, which is composed of mandibular and postcranial fragments and a left caniniform process with the triangular morphology characteristic of *Angonisaurus* (Hancox et al., 2013). As such, NHMUK PV R9732 remains the primary source for comparisons concerning the genus.

Hancox et al. (2013) listed the following characters supporting referral of BP/1/5530 and BP/1/5531 to *Angonisaurus*: no strong break in slope between intertemporal bar and frontals;

postorbitals do not extend the full length of the intertemporal bar to reach the squamosals; parietals widely exposed in dorsal view with well-developed mid-line groove; interparietal (also known and herein referred to as the postparietal) makes a moderate contribution to skull roof and meets the parietals along an interdigitated suture. As they noted, however, none of these characters alone is autapomorphic for *Angonisaurus*; rather this constitutes a differential diagnosis, which they argued can be used to distinguish *Angonisaurus* from other Triassic dicynodonts. A strong break in slope along the length of the intertemporal bar is a characteristic feature of *Kannemeyeria* and its allies (which may or may not constitute a monophyletic Kannemeyeriidae; see, e.g., Kammerer et al., 2011; Olroyd et al., 2018; Angielczyk et al., 2018); it is usually not present in shansiodontid and stahleckeriid kannemeyeriiforms. Restriction of the postorbitals to the anterior wall of the temporal fenestra is present in all shansiodontids and several stahleckeriids (*Ischigualastia*, *Jachaleria*, *Placerias*, and *Moghreberia*). Broad exposure of the parietals dorsally is typically present in stahleckeriids (albeit not *Ischigualastia* and *Jachaleria*), and exposure in a median groove is present in at least *Sangusaurus* (Angielczyk et al., 2018) and *Zambiasaurus* (based on NHMUK PV R9021). A substantial contribution of the postparietal to the posterior section of the intertemporal bar is probably more broadly distributed in kannemeyeriiforms than currently recognized; a triangular anterior process of the postparietal separating the parietals is definitely present in *Sangusaurus* (based on NMT RB42), and a contact between this process and an interdigitated mid-parietal suture is present in *Dolichuranus* (based on BP/1/4570). Taken as a whole, then, the aforementioned character list is present more broadly than argued by Hancox et al. (2013): even in combination they only characterize Stahleckeriidae in general.

While referral of BP/1/5530 and BP/1/5531 to *Angonisaurus* was reasonable at the time given the extent of the preserved material, the nearly-complete morphology of BP/1/8208 reveals that this taxon differs markedly from *Angonisaurus cruickshanki* (Fig. 10) and cannot be considered the same taxon. The most important point of distinction between these taxa is in the intertemporal region, which is also preserved in BP/1/5530 and BP/1/5531, but poorly so in BP/1/5531, making it understandable that differences between BP/1/5530 and NHMUK PV R9732 could be interpreted as individual or taphonomic variation in the absence of well-preserved material (like BP/1/8208) showing the same morphology. In *Angonisaurus cruickshanki*, the intertemporal bar is broad anteriorly and gradually tapers towards the occiput. The parietals are exposed dorsally in a narrow median groove posterior to the pineal foramen that is of equal width throughout the length of the bar and extends to the occiput; the parietal contributions to the posterior wall of the temporal fenestra also form tall edges lateral to this groove. The postparietal of *Angonisaurus* occupies a relatively posterior portion of the intertemporal bar and only flares laterally above the occiput. In contrast to the above, in *Ufudocyclops mukanelai*, the intertemporal bar is distinctly 'X'-shaped, broad both anteriorly and posteriorly and sharply constricted at midlength (more so in BP/1/5530 than BP/1/5531 or BP/1/8208, but clearly present in all three). The parietals of *Ufudocylops* are not exposed dorsally in a midline groove: they are restricted to a broad, roughly triangular-to-trapezoidal median depression immediately posterior to the pineal foramen (making up the space between the anterior legs of the 'X'). The postparietal is present in a relatively anterior position on the intertemporal bar of *Ufudocyclops* compared to *Angonisaurus*, and bears raised, laterally-flaring paired swellings (most evident in BP/1/5530) taking up an extensive portion of the pre-occipital length of the bar (they form the posterior legs of the 'X'). The absence of a prepariental, which

Hancox et al. (2013) also argued unites BP/1/5530 and BP/1/5531 with *Angonisaurus*, is a rare occurrence among dicynodonts, but is also the case in *Stahleckeria* (Maisch, 2001), so cannot be considered autapomorphic.

In addition to intertemporal morphology, several other autapomorphies readily distinguish *Ufudocyclops mukanelai* from *Angonisaurus cruickshanki*. The nasal bosses of *Ufudocyclops* are unique among kannemeyeriiforms and much more closely resemble those of Permian cryptodonts like *Rhachiocephalus*, being large, highly discrete, ovoid, and separated by a broad, unornamented median span of premaxilla and nasals. Distinct nasal bosses overhanging the external nares are also present in shansiodontids among Triassic taxa, but are usually very small. The large nasal bosses of the Russian shansiodontid *Rhinodicynodon gracile* are comparable in proportions to those of *Ufudocyclops*, but in that taxon are much more closely-spaced, with rugosity extending onto the dorsal surface of the nasals (based on PIN 1579/50). As regards *Angonisaurus*, although the anterior snout of NHMUK PV R9732 is not well-preserved, it displays the typical kannemeyeriiform morphology of a generally rugose, expanded nasal surface extending across the dorsal margin of the snout. *Angonisaurus cruickshanki* also lacks the laterally-expanded jugal plate extending beneath the orbit that is characteristic of *Ufudocyclops*. Although the zygomatic arch is also somewhat poorly preserved in NHMUK PV R9732, sutural boundaries are visible on the right side of the zygoma and show a typical kannemeyeriiform morphology, in which the jugal is restricted to a thin strip laterally lining the ventral margin of the orbit.

The morphology of the caniniform process in *Ufudocyclops* is not unique to this taxon; similar caniniforms are present in other tuskless kannemeyeriiforms (e.g., *Wadiasaurus*, *Ischigualastia*). However, the caniniform process in *Angonisaurus cruickshanki* is very

distinctive (permitting referral of even highly incomplete specimens like NMT RB155), forming a broad-based triangle with a posteroventrally-directed tip coming to a distinct point (Fig. 10D). The caniniform process of *Ufudocyclops* (preserved to varying extents in all three specimens of this taxon) has the more typical anteroventrally-directed orientation seen in most other stahleckeriids, and terminates in a blunter, more rounded tip. In palatal view, the caniniform process of *Angonisaurus* is also anteroposteriorly and transversely thicker than in *Ufudocyclops*, with a more distinctly triangular shape. The morphology of the basal tubera is also distinct between *Angonisaurus* and *Ufudocyclops*: in the former it is more semicircular, with markedly inflated edges as in *Kannemeyeria* or *Dolichuranus*, while in the latter it is anteroposteriorly elongate and thinner as in *Stahleckeria* (and nearing the quadrangular, close-packed morphology of *Ischigualastia* and *Jachaleria*).

Sidor et al. (2014) referred an additional specimen (UWBM 95538, a partial left squamosal) from the upper Fremouw Formation of Antarctica to *Angonisaurus* sp. Although extremely fragmentary, they considered this specimen referable to *Angonisaurus* on the basis of its thickened, robust squamosal margin and the near-vertical orientation of the quadrate ramus of the squamosal. They tentatively considered the thickened squamosal to be autapomorphic for *Angonisaurus* (a near-vertical quadrate ramus of the squamosal is present more broadly in stahleckeriids, and is especially prominent in *Ischigualastia* and *Jachaleria*; worth noting is that this ramus is curved rather than vertical in BP/1/8208). A thickened squamosal margin is indeed present in NHMUK PV R9732 and BP/1/8208 in addition to UWBM 95538. However, distinct thickening along the squamosal margin is also present in *Jachaleria* (based on PVL 3841 and UFRGS PV-0151-T), and we do not consider this feature autapomorphic for *Angonisaurus* (a greatly expanded zygomatic ramus of the squamosal is also present in *Moghreberia* and

Placerias, but in those taxa takes the form of a more laminar dorsoventral expansion and not just a thickening of the bone surface). At present, we consider UWBM 95539 identifiable only as Stahleckeriidae indet. (although the co-occurrence of any member of this family with *Cynognathus*, as in the upper Fremouw Formation, is intriguing).

Thickening of the circumorbital region, in the form of bosses forming the orbital rim of the prefrontal and postorbital, is also shared between *Ufudocyclops* and *Angonisaurus* (these features were not considered present in BP/1/5530 and BP/1/5531 by Hancox *et al*. [2013] because of poor preservation, but are very well developed in BP/1/8208). However, here too this character is more broadly distributed among stahleckeriids: some kind of rugosity on the postorbital bar is present in nearly all taxa, and restriction to a boss-like eminence at the posterodorsal corner of the orbit is also the case in *Stahleckeria* (based on GPIT/RE/7107) and *Jachaleria* (based on UFRGS PV-0151-T). Prefrontal bosses or at least raised eminences at the anteroventral corner of the orbit are also widespread among kannemeyeriiforms in general.

In summary, the three dicynodont specimens under discussion from Subzone C of the *Cynognathus* AZ (BP/1/5530, BP/1/5531, BP/1/8208) differ from *Angonisaurus cruickshanki* in a number of consistent features, several of which are unique among kannemeyeriiforms. Although they share some characters with *Angonisaurus* (tusklessness, absence of a preparietal, thickened edge of the zygomatic ramus of the squamosal, prefrontal and postorbital bosses, postorbital restricted to the anterior wall of the temporal fenestra, broad exposure of the parietal in the intertemporal bar), all of these characters are more widely distributed within Stahleckeriidae. In light of the aforementioned autapomorphies, and the fact that we do not recover the Subzone C material as sister-taxon to *Angonisaurus cruickshanki* in our phylogenetic

analysis, we consider the establishment of a new genus and species for the Subzone C specimens to be justified.

Early Diversity of Stahleckeriidae

Stahleckeriids are the latest-surviving dicynodonts (definitively reaching the Norian and possibly the Rhaetian: Dzik et al., 2008; Kent et al., 2014; Kammerer, 2018; Sulej and Niedźwiedzki, 2019) and are usually thought of as being components of primarily Late Triassic faunal assemblages (Kammerer et al., 2013). However, fragmentary members of both stahleckeriid subclades (Placeriinae and Stahleckeriinae) are known from possible Middle Triassic deposits in Zambia (i.e., the Ntawere Formation, which yields *Zambiasaurus submersus* and *Sangusaurus edentatus*; Angielczyk et al., 2014; Kammerer et al., 2018). Based on the recent discovery of more complete materials of *Sangusaurus* from the middle-upper Lifua Member of the Manda Beds of Tanzania (referable to *S. parringtonii*), this genus is now robustly supported as a stahleckeriine stahleckeriid (Angielczyk et al., 2018). *Angonisaurus* has long been a problematic taxon in dicynodont phylogeny (Kammerer et al., 2011), but similarities between it and stahleckeriids have long been recognized (Hancox, 1998; Vega-Dias et al., 2004; Surkov et al., 2005) and recent phylogenetic analyses (Angielczyk and Kammerer, 2017; Angielczyk et al., 2018; Kammerer, 2018; Olroyd et al., 2018) consistently support a position for it as the sister-taxon of Stahleckeriidae sensu Kammerer et al. (2013).

The description of *Ufudocyclops mukanelai* adds another Middle Triassic stahleckeriid to the taxa mentioned above, potentially the earliest known, suggesting that the diversification of this clade was well under way by the Anisian, concurrent with the diversification of shansiodontid and kannemeyeriid kannemeyeriiforms. As such, the prevalence of Late Triassic

stahleckeriids may simply reflect long-lasting continuation of this radiation, rather than a 'slow fuse' requiring the extinction of earlier kannemeyeriiform groups to diversify. With this said, the absence of the previously-abundant *Kannemeyeria simocephalus* in *Cynognathus* Subzone C does suggest that some local turnover in large herbivore niches was benefiting stahleckeriids: *Ufudocyclops* is similar in size to *Kannemeyeria* and likely would have occupied an ecologically comparable role.

Although the Early Triassic kannemeyeriiform record is so poor that the possibility cannot be discounted, we do not consider stahleckeriids to be present in the Early Triassic based on known material. Maisch and Matzke (2014) described a dicynodont from the Early Triassic of China (*Sungeodon kimkraemerae*) that they considered to be stahleckeriid. However, the holotype of *Sungeodon* shows no stahleckeriid synapomorphies, and much more closely resembles various Chinese kannemeyeriid taxa (e.g., *Sinokannemeyeria*, *Parakannemeyeria*) and even some non-kannemeyeriid dicynodontoids (e.g., *Daptocephalus*, *Turfanodon*) (Kammerer, pers. obs.)

Biostratigraphic Implications

The removal of BP/1/5530 and BP/1/5531 from referral to *Angonisaurus* eliminates one of the most important biostratigraphic links between *Cynognathus* Subzone C and the Lifua Member of the Tanzanian Manda Beds. Here, we recognize these specimens as referable to a distinct kannemeyeriiform taxon, *Ufudocyclops mukanelai*, which seems to be restricted to the Subzone C deposits of South Africa. The only other dicynodont record from Subzone C, a complete skull, partial jaws, and associated postcranium (BP/1/5532) that Hancox et al. (2013) referred to *Shansiodon* sp., does not provide any clear biostratigraphic link to the Manda Beds: although shansiodontid remains (*Tetragonias njalilus*) are known from the Lifua Member, this

family is geographically (and apparently stratigraphically) widespread, ranging through (possibly) Olenekian–Ladinian rocks in South America, Russia, and China in addition to southern Africa (Domnanovich and Marsicano, 2012). All other specimens of *Shansiodon* are from the Chinese *Sinokannemeyeria* Fauna, which has been dated as late Anisian based on U-Pb zircon analysis (Liu et al., 2018). We also consider the Antarctic specimen referred to *Angonisaurus* by Sidor et al., (2014) to be identifiable only as an indeterminate stahleckeriid, and caution against using this specimen to correlate the upper Fremouw Formation with *Cynognathus* Subzone C and the Manda Beds.

With *Angonisaurus* no longer considered part of the Subzone C fauna, this leaves only the trirachodontid eucynodont *Cricodon metabolus* to correlate the South African assemblage with the Manda Beds. Crompton (1955) originally described *Cricodon metabolus* on the basis of a fragmentary skull and skeleton. Abdala et al. (2005a) referred several partial trirachodontid skulls from *Cynognathus* Subzone C to *C. metabolus*, but these specimens were generally poorly preserved, limiting comparisons with the Tanzanian type material. Sidor and Hopson (2018) recently described new, better-preserved material of this taxon from the Ntawere Formation of Zambia and provided an updated list of referred specimens of *C. metabolus*, but did not include the South African specimens in their hypodigm, noting only that they could "possibly" be *Cricodon*. Detailed comparisons with the Subzone C trirachodontid specimens and the type material is required to assess this referral; at present we concur with Sidor and Hopson (2018) in considering it possible, but needing additional study.

The presence of a distinct dicynodont fauna in *Cynognathus* Subzone C from that seen elsewhere in the southern African Triassic (i.e., Omingonde Formation of Namibia, Manda Beds of Tanzania, and Ntawere Formation of Zambia), coupled with endemic temnospondyl species

(Damiani and Hancox, 2003; Damiani, 2008) and only a questionable link in the eucynodont record, suggests that this assemblage is not part of a broadly-distributed Middle Triassic African fauna. Rather than being a southern extension of faunas best known from Tanzanian and Zambian deposits (as argued by Abdala et al., 2005; Hancox et al., 2013; Peecook et al., 2018), based on known fossils it seems to represent a distinct local fauna restricted to the Karoo Basin (although whether this is due to geographic or temporal separation from these other faunas is uncertain). This suggests that even by the Middle Triassic, tetrapod faunas had begun to exhibit high levels of regionalization, perhaps to an even greater degree than previously (Sidor et al., 2013) proposed.

Finally, it should be mentioned that the traditional Middle Triassic age for the *Cynognathus* AZ was questioned by Ottone et al. (2014), who presented SHRIMP U-Pb zircon dates indicating that the Puesto Viejo Group (which contains the *Cynognathus*/*Diademodon*-bearing Río Seco de la Quebrada Formation) is actually Carnian. Based on this result, they argued that either the trans-Gondwanan '*Cynognathus* Fauna' lasted substantially longer than previously thought (Early–Late Triassic) or that the Burgersdorp Formation represents a much later series of deposits than the rest of the Beaufort Group. Although few radioisotopic dates are currently available for comparable Triassic tetrapod assemblages, Liu et al. (2018) recently demonstrated that the *Sinokannemeyeria* Fauna in China is late Anisian in age using high-resolution CA-TIMS U-Pb dating. The *Sinokannemeyeria* Fauna has often been considered a northern hemisphere equivalent of the *Cynognathus* Fauna (Sun, 1980), and although historically this correlation was based on vague, clade-level comparisons (e.g., shared abundance of kannemeyeriid dicynodonts and erythrosuchid archosauriforms), the discovery of the typical *Sinokannemeyeria* Fauna genus *Shansiodon* in Subzone C of the *Cynognathus* AZ (Hancox et

al., 2013) suggests that this comparison was not totally unfounded. This result accords with prevailing hypotheses concerning the age of the *Cynognathus* AZ, in which Subzone A is considered late Olenekian and B and C are considered early and late Anisian (Hancox, 2000). Here, we consider a Carnian age for any of the *Cynognathus* AZ unlikely, although we recognize that more radioisotopic dates for Karoo strata and *Cynognathus*-bearing assemblages worldwide are needed to resolve this issue. As the case of *Ufudocyclops* shows, tetrapod distribution in the Triassic is a complex topic, and existing biostratigraphic schemes may not be as well supported as they appear.

ACKNOWLEDGMENTS

Thanks to D. Osborne, owner of the farm Thala on which the holotype BP/1/8208 was found. We thank all members of the 2014 and 2017 *Cynognathus* C field teams: E. Bordy, D. Cashmore, M. Day, K. Dollman, E. Dunne, M. Ezcurra, P. Godoy, A. Jones, B. McPhee, J. Neenan, and R. Sookias. CFK thanks the many curators and collections managers who have provided access to comparative materials, especially S. Jirah (ESI), I. Werneburg (GPIT), P. Barrett (NHMUK), V. Golubev (PIN), the late J. Powell (PVL), and C. Schultz (UFRGS). We thank C. Mdekazi for consultation on the genus name of the new dicynodont, K. Angielczyk, J. Fröbisch, B. Peecook, and T. Sulej for their helpful reviews, and A. Huttenlocker for his work as editor. Funding for fieldwork was provided by a Marie Curie Career Integration Grant (630123 to RJB), the NRF African Origins Platform (98800 to JNC), and by Palaeontological Scientific Trust (JNC).

LITERATURE CITED

Abdala, F., and R. M. H. Smith. 2009. A Middle Triassic cynodont fauna from Namibia and its implications for the biogeography of Gondwana. Journal of Vertebrate Paleontology 29:837–851.

Abdala, F., and A. M. Ribeiro. 2010. Distribution and diversity patterns of Triassic cynodonts (Therapsida, Cynodontia) in Gondwana. Palaeogeography, Palaeoclimatology, Palaeoecology 286:202–217.

Abdala, F., P. J. Hancox, and J. Neveling. 2005a. Cynodonts from the uppermost Burgersdorp Formation, South Africa, and their bearing on the biostratigraphy and correlation of the Triassic *Cynognathus* Assemblage Zone. Journal of Vertebrate Paleontology 25:192–199.

Abdala, F., J. Neveling, and B. S. Rubidge. 2005b. A new cynodont from the base of the *Cynognathus* Assemblage Zone (Lower Triassic) of the Karoo Basin: wrong teeth or wrong skull?; p. 31 in R. J. Pankhurst and G. D. Veiga (eds). Gondwana 12: Geological and biological heritage of Gondwana, Abstracts, Academia Nacional de Ciencias, Cordoba, Argentina.

Angielczyk, K. D., and C. F. Kammerer. 2017. The cranial morphology, phylogenetic position and biogeography of the upper Permian dicynodont *Compsodon helmoedi* van Hoepen (Therapsida, Anomodontia). Papers in Palaeontology 3:513–545.

Angielczyk, K. D., P. J. Hancox, and A. Nabavizadeh. 2018. A re-description of the Triassic kannemeyeriiform dicynodont *Sangusaurus* (Therapsida, Anomodontia), with an analysis of its feeding system. Society of Vertebrate Paleontology Memoir 17:189–227.

Angielczyk, K. D., J. S. Steyer, C. A. Sidor, R. M. H. Smith, R. L. Whatley, and S. Tolan. 2014. Permian and Triassic dicynodont (Therapsida: Anomodontia) faunas of the Luangwa Basin,

Zambia: taxonomic update and implications for dicynodont biogeography and biostratigraphy; pp. 93–138 in C. F. Kammerer, K. D. Angielczyk, and J. Fröbisch (eds) Early Evolutionary History of the Synapsida. Springer, Dordrecht.

Bonaparte, J. F. 1966. Chronological survey of the tetrapod-bearing Triassic of Argentina. Breviora 251:1–13.

Bonaparte, J. F. 1969. *Cynognathus minor* n. sp. (Therapsida–Cynodontia). Nueva evidencia de vinculación faunística Afro-Sudamericana a principios del Triásico; pp. 273–382 in Gondwana Stratigraphy, I.U.G.S. Coloquio Mar del Plata. Imprimerie Louis-Jean, Gap.

Brink, A. S. 1963. Two cynodonts from the Ntawere Formation in the Luangwa Valley of Northern Rhodesia. Palaeontologia africana 8:77–96.

Broom, R. 1905. On the use of the term Anomodontia. Records of the Albany Museum 1:266–269.

Catuneanu, O., H. Wopfner, P. G. Eriksson, B. Cairncross, B. S. Rubidge, R. M. H. Smith, and P. J. Hancox. 2005. The Karoo basins of south-central Africa. Journal of African Earth Sciences 43:211–253.

Colbert, E. H. 1991. Mesozoic and Cainozoic tetrapod fossils from Antarctica; pp. 568–587 in R. J. Tingey (ed.) The Geology of Antarctica. Clarendon Press, Oxford.

Cox, C. B., and J.-L. Li. 1983. A new genus of Triassic dicynodont from East Africa and its classification. Palaeontology 26:389–406.

Crompton, A. W. 1955. On some Triassic cynodonts from Tanganyika. Proceedings of the Zoological Society of London 1125:617–669.

Cruickshank, A. R. I. 1965. On a specimen of the anomodont reptile *Kannemeyeria latifrons* (Broom) from the Manda Formation of Tanganyika, Tanzania. Proceedings of the Linnean Society of London 176:149–157.

Damiani, R. J. 2008. A giant skull of the temnospondyl *Xenotosuchus africanus* from the Middle Triassic of South Africa and its ontogenetic implications. Acta Palaeontologica Polonica 53:75–84.

Damiani, R. J., and P. J. Hancox. 2003. New mastodonsaurid temnospondyls from the *Cynognathus* Assemblage Zone (Upper Beaufort Group; Karoo Basin) of South Africa. Journal of Vertebrate Paleontology 23:54–66.

Domnanovich, N. S., and C. A. Marsicano. 2012. The Triassic dicynodont *Vinceria* (Therapsia, Anomodontia) from Argentina and a discussion on basal Kannemeyeriiformes. Geobios 45:173–183.

Dzik, J., T. Sulej, and G. Niedźwiedzki. 2008. A dicynodont-theropod association in the latest Triassic of Poland. Acta Palaeontologica Polonica 53:733–738.

Goloboff, P. A., C. I. Mattoni, and A. S. Quinteros. 2006. Continuous characters analyzed as such. Cladistics 22:589–601.

Goloboff, P. A., J. S. Farris, and K. C. Nixon. 2008. TNT, a free program for phylogenetic analysis. Cladistics 24:774–786.

Gower, D. J., P. J. Hancox, J. Botha-Brink, A. G. Sennikov, and R. J. Butler. 2014. A new species of *Garjainia* Ochev, 1958 (Diapsida: Archosauriformes: Erythrosuchidae) from the Early Triassic of South Africa. PLoS ONE 9(11):e111154.

Hammer, W. R. 1995. New therapsids from the upper Fremouw Formation (Triassic) of Antarctica. Journal of Vertebrate Paleontology 15:105–112.

Hancox, P. J. 1998. A stratigraphic, sedimentological and palaeoenvironmental synthesis of the Beaufort-Molteno contact in the Karoo Basin. Unpublished PhD thesis, University of the Witwatersrand, Johannesburg.

Hancox, P. J. 2000. The continental Triassic of South Africa. Zentralblatt für Geologie und Paläontologie Teil I, Heft 11–12, 1998:105–112.

Hancox, P. J., and B. S. Rubidge. 1996. The first specimen of the mid-Triassic dicynodont *Angonisaurus* from the Karoo of South Africa: implications for the dating and biostratigraphy of the *Cynognathus* Assemblage Zone, Upper Beaufort Group. South African Journal of Science 92:391–392.

Hancox, P. J., K. D. Angielczyk, and B. S. Rubidge. 2013. *Angonisaurus* and *Shansiodon*, dicynodonts (Therapsida, Anomodontia) from Subzone C of the *Cynognathus* Assemblage Zone (Middle Triassic) of South Africa. Journal of Vertebrate Paleontology 33:655–676.

Hancox, P. K., M. A. Shishkin, B. S. Rubidge, and J. W. Kitching. 1995. A threefold subdivision of the *Cynognathus* Assemblage Zone (Beaufort Group, southern Africa) and its palaeogeographical implications. South African Journal of Science 91:143–144.

Kammerer, C. F. 2016. Systematics of the Rubidgeinae (Therapsida: Gorgonopsia). PeerJ 4:e1608.

Kammerer, C. F. 2018. The first skeletal evidence of a dicynodont from the lower Elliot Formation of South Africa. Palaeontologia africana 52:102–128.

Kammerer, C. F., K. D. Angielczyk, and J. Fröbisch. 2011. A comprehensive taxonomic revision of *Dicynodon* (Therapsida, Anomodontia) and its implications for dicynodont phylogeny, biogeography, and biostratigraphy. Society of Vertebrate Paleontology Memoir 11:1–158.

Kammerer, C. F., K. D. Angielczyk, and J. Fröbisch. 2013. On the validity and phylogenetic position of *Eubrachiosaurus browni*, a kannemeyeriiform dicynodont (Anomodontia) from Triassic North America. PLoS ONE 8(5):e64203.

Kammerer, C. F., K. D. Angielczyk, and J. Fröbisch. 2015. Redescription of the geikiid *Pelanomodon* (Therapsida, Dicynodontia), with a reconsideration of '*Propelanomodon*'. Journal of Vertebrate Paleontology e0130408.

Kammerer, C. F., K. D. Angielczyk, and S. J. Nesbitt. 2018. Novel hind limb morphology in a kannemeyeriiform dicynodont from the Manda Beds (Songea Group, Ruhuhu Basin) of Tanzania. Society of Vertebrate Paleontology Memoir 17:178–188.

Kent, D. V., P. Santi Malnis, C. E. Colombi, O. A. Alcober, and R. N. Martínez. 2014. Age constraints on the dispersal of dinosaurs in the Late Triassic from magnetochronology of the Los Colorados Formation (Argentina). Proceedings of the National Academy of Sciences of the United States of America 111:7958–7963.

Keyser, A. W. 1973. A new Triassic vertebrate fauna from South West Africa. Palaeontologia africana 16:1–15.

Keyser, A. W. 1979. A review of the biozonation of the Beaufort Group in the Karoo basin of South Africa. Geological Society of South Africa, Abstracts of 1979 Geological Congress 2:13–31.

Keyser, A. W., and A. R. I. Cruickshank. 1979. The origins and classification of Triassic dicynodonts. Transactions of the Geological Society of South Africa 82:81–108.

Keyser, A. W., and R. M. H. Smith. 1978. Vertebrate bizonation of the Beaufort Group with special reference to the western Karoo Basin. Annals of the Geological Survey, Republic of South Africa 12:1–35.

King, G. A. 1988. Anomodontia. Handbuch der Paläoherpetologie, 17C. Gustav Fischer Verlag, Stuttgart, 174 pp.

Kitching, J. W. 1984. A reassessment of the biozonation of the Beaufort Group. Paleo News 4:12–13.

Lehman, J.-P. 1961. Dicynodontia; pp. 287-351 in J.-P. Piveteau (ed.) Traité de Paléontologie, VI, Mammifères, Vol 1.: Origine Reptilienne Èvolution. Masson et Cie, Paris.

Liu, J., J. Ramezani, L. Li, Q.-H. Shang, G.-H. Xu, Y.-Y. Wang, and J.-S. Yang. 2018. High-precision temporal calibration of Middle Triassic vertebrate biostratigraphy: U-Pb zircon constraints for the *Sinokannemeyeria* Fauna and *Yonghesuchus*. Vertebrata PalAsiatica 56 :16–24.

Maisch, M. W. 2001. Observations on Karoo and Gondwana vertebrates. Part 2: A new skull-reconstruction of *Stahleckeria potens* von Huene, 1935 (Dicynodontia, Middle Triassic) and reconsideration of kannemeyeriiform phylogeny. Neues Jahrbuch für Geologie und Paläontologie Abhandlungen 220:127–152.

Martinelli, A. G., M. de la Fuente, and F. Abdala. 2009. *Diademodon tetragonus* Seeley, 1894 (Therapsida: Cynodontia) in the Triassic of South America and its biostratigraphic implications. Journal of Vertebrate Paleontology 29:852–862.

Neveling, J., P. J. Hancox, and B. S. Rubidge. 2005. Biostratigraphy of the lower Burgersdorp Formation (Beaufort Group; Karoo Supergroup) of South Africa—implications for the stratigraphic ranges of early Triassic tetrapods. Palaeontologia africana 41:81–87.

Olroyd, S. L., C. A. Sidor, and K. D. Angielczyk. 2018. New materials of the enigmatic dicynodont *Abajudon kaayai* (Therapsida, Anomodontia) from the lower Madumabisa Mudstone Formation, middle Permian of Zambia. Journal of Vertebrate Paleontology e1403442.

Ottone, E. G., M. Monti, C. A. Marsicano, M. S. del la Fuente, M. Naipauer, R. Armstrong, and A. C. Mancuso. 2014. A new Late Triassic age for the Puesto Viejo Group (San Rafael depocenter, Argentina): SHRIMP U-Pb zircon dating and biostratigraphic correlations across southern Gondwana. Journal of South American Earth Sciences 56:186–199.

Osborn, H. F. 1903. On the primary division of the Reptilia into two sub-classes, Synapsida and Diapsida. Science 17:275–276.

Owen, R. 1860. On the orders of fossil and recent Reptilia, and their distribution in time. Report of the Twenty-Ninth Meeting of the British Association for the Advancement of Science 1859:153–166.

Peecook, B. R., J. S. Steyer, N. J. Tabor, and R. M. H. Smith. 2018. Updated geology and vertebrate paleontology of the Triassic Ntawere Formation of northeastern Zambia, with special emphasis on the archosauromorphs. Society of Vertebrate Paleontology Memoir 17:8–38.

Ray, S. 2005. *Lystrosaurus* (Therapsida, Dicynodontia) from India: taxonomy, relative growth and cranial dimorphism. Journal of Systematic Palaeontology 3:203–221.

Renaut, A. J., and P. J. Hancox. 2001. Cranial description and taxonomic re-evaluation of *Kannemeyeria argentinensis* (Therapsida: Dicynodontia) Palaeontologia africana 37:81–91.

Rubidge, B. S. (ed.) 1995. Biostratigraphy of the Beaufort Group (Karoo Supergroup). South African Committe for Stratigraphy, Biostratigraphic Series 1:1–46.

Sennikov, A. G. 1996. Evolution of the Permian and Triassic tetrapod communities of Eastern Europe. Palaeogeography, Palaeoclimatology, Palaeoecology. 120:331–351.

Sennikov, A. G., and V. K. Golubev. 2006. Vyazniki biotic assemblage of the terminal Permian. Paleontological Journal 40:S475–S481.

Shishkin, M. A., B. S. Rubidge, and P. J. Hancox, P. J. 1995. Vertebrate biozonation of the Upper Beaufort Series of South Africa—a new look on correlation of the Triassic biotic events in Euramerica and southern Gondwana; pp. 39–41 in Sixth Symposium on Mesozoic Terrestrial Ecosystems. China Press, Beijing.

Sidor, C. A., and J. A. Hopson. 2018. *Cricodon metabolus* (Cynodontia: Gomphodontia) from the Triassic Ntawere Formation of northeastern Zambia: patterns of tooth replacement and a systematic review of the Trirachodontidae. Society of Vertebrate Paleontology Memoir 17:39–64.

Sidor, C. A., and S. J. Nesbitt. 2018. Introduction to vertebrate and climatic evolution in the Triassic rift basins of Tanzania and Zambia. Society of Vertebrate Paleontology Memoir 17:1–7.

Sidor, C. A., R. M. H. Smith, A. K. Huttenlocker, and B. R. Peecook. 2014. New Middle Triassic tetrapods from the upper Fremouw Formation of Antarctica and their depositional setting. Journal of Vertebrate Paleontology 34:793–801.

Sidor, C. A., D. A. Vilhena, K. D. Angielczyk, A. K. Huttenlocker, S. J. Nesbitt, B. R. Peecook, J. S. Steyer, R. M. H. Smith, and L. A. Tsuji. 2013. Provincialization of terrestrial faunas following the end-Permian mass extinction. Proceedings of the National Academy of Sciences of the United States of America 110:8129–8133.

Smith, R. M. H., and R. Swart. 2002. Changing fluvial environments and vertebrate taphonomy in response to climate drying in a mid-Triassic rift valley fill: the Omingonde Formation (Karoo Supergroup) of Central Namibia. Palaios 17:249–267.

Smith, R.M.H., B.S. Rubidge, and M. van der Walt. 2012. Therapsid biodiversity patterns and palaeoenvironments of the Karoo Basin, South Africa; pp. 31–62 in A. Chinsamy-Turan (ed.), Forerunners of Mammals: Radiation, Histology, Biology. Indiana University Press, Bloomington.

Smith, R. M. H., C. A. Sidor, K. D. Angielczyk, S. J. Nesbitt, and N. J. Tabor. 2018. Taphonomy and paleoenvironments of Middle Triassic bone accumulations in the Lifua Member of the

Manda Beds, Songea Group (Ruhuhu Basin), Tanzania. Society of Vertebrate Paleontology Memoir 17:65–79.

Sulej, T., and Niedźwiedzki, G. 2019. An elephant-sized Late Triassic synapsid with erect limbs. Science 363:78–80.

Sullivan, C. R., and R. R. Reisz. 2005. Cranial anatomy and taxonomy of the Late Permian dicynodont *Diictodon*. Annals of Carnegie Museum 74:45–75.

Sun, A. 1980. Late Permian and Triassic terrestrial tetrapods of north China. Vertebrata PalAsiatica 18:100–110.

Surkov, M. V., N. N. Kalandadze, and M. J. Benton. 2005. *Lystrosaurus georgi*, a dicynodont from the Lower Triassic of Russia. Journal of Vertebrate Paleontology 25:402–413.

Vega-Dias, C., M. W. Maisch, and C. L. Schultz. 2004. A new phylogenetic analysis of Triassic dicynodonts (Therapsida) and the systematic position of *Jachaleria candelariensis* from the Upper Triassic of Brazil. Neues Jahrbuch für Geologie und Paläontologie Abhandlungen 231:145–166.

Wynd, B. M., B. R. Peecook, M. R. Whitney, and C. A. Sidor. 2018. The first occurrence of *Cynognathus* in Tanzania and Zambia, with biostratigraphic implications for the age of Triassic strata in southern Pangea. Society of Vertebrate Paleontology Memoir 17:228–239.

Submitted December 14, 2018; revisions received February 18, 2019; accepted Month DD, YYYY.

FIGURE CAPTIONS

FIGURE 1. Geological context for BP/1/8208, holotype of *Ufudocyclops mukanelai*, showing position in stratigraphic section where specimen was discovered and site of the type locality. [Intended for page width]

FIGURE 2. Photographs of BP/1/8208, holotype of *Ufudocyclops mukanelai*. Anterior fragment of premaxilla in **A**, anterior and **B**, posterior views. **C**, skull in anterior view with snout tip removed to show internal trabecular structure of premaxilla. **D**, skull in anterior view with snout tip in place. **E**, skull in left lateral view. Scale bars equal 1 cm. [Intended for page width]

FIGURE 3. Photograph and interpretive drawing of BP/1/8208, holotype of *Ufudocyclops mukanelai*, in dorsal view. **Abbreviations**: **fr**, frontal; **j**, jugal; **mx**, maxilla; **na**, nasal; **op**, opisthotic; **pa**, parietal; **pf**, pineal foramen; **pmx**, premaxilla; **po**, postorbital; **pop**, postparietal; **pr?**, prootic; **prf**, prefrontal; **sq**, squamosal. Gray indicates matrix; dotted lines indicate uncertain sutural boundaries or missing bone. Scale bar equals 5 cm. [Intended for page width]

FIGURE 4. Photograph and interpretive drawing of BP/1/8208, holotype of *Ufudocyclops mukanelai*, in right lateral view. **Abbreviations**: **af**, fossa for M. adductor mandibulae externus lateralis; **cp**, caniniform process of maxilla; **fo**, fenestra ovalis; **fr**, frontal; **j**, jugal; **la**, lacrimal; **mx**, maxilla; **na**, nasal; **pa**, parietal; **pmx**, premaxilla; **po**, postorbital; **pr?**, prootic; **prf**, prefrontal; **pt**, pterygoid; **q**, quadrate; **smx**, septomaxilla; **sq**, squamosal. Gray indicates matrix; dotted lines indicate missing bone. Scale bar equals 5 cm. [Intended for page width]

FIGURE 5. Photograph and interpretive drawing of BP/1/8208, holotype of *Ufudocyclops mukanelai*, in ventral view. **Abbreviations**: **apr**, anterior palatal ridge; **apt**, anterior pterygoid ramus; **bt**, basal tuber; **fo**, fenestra ovalis; **j**, jugal; **mpr**, median palatal ridge; **mx**, maxilla; **na**, nasal; **oc**, occipital condyle; **pal**, palatine; **pap**, paroccipital process of opisthotic; **pfo**, palatine foramen; **pmx**, premaxilla; **q**, quadrate; **qpt**, quadrate (=posterior) pterygoid ramus; **sq**, squamosal; **v**, vomer. Gray indicates matrix; patterning indicates broken edge of maxillary bone; dotted lines indicate uncertain sutural boundaries or missing bone. Scale bar equals 5 cm. [Intended for page width]

FIGURE 6. Photograph and interpretive drawing of BP/1/8208, holotype of *Ufudocyclops mukanelai*, in occipital view. **Abbreviations**: **bt**, basal tuber; **fm**, foramen magnum; **oc**, occipital condyle; **pap**, paroccipital process of opisthotic; **pe**, periotic; **ptf**, post-temporal fenestra; **pop**, postparietal; **sq**, squamosal; **sqr**, squamosal ridge; **ta**, tabular. Gray indicates matrix; dotted lines indicate uncertain sutural boundaries. Scale bar equals 5 cm. [Intended for page width]

FIGURE 7. BP/1/5530, referred specimen of *Ufudocyclops mukanelai*, in **A**, dorsal (anterior is right) and **B**, left lateral views with **C**, **D** interpretive drawings. **Abbreviations**: **fr**, frontal; **j**, jugal; **la**, lacrimal; **lf**, lacrimal foramen; **na**, nasal; **pa**, parietal; **pd**, parietal depression; **pf**, pineal foramen; **po**, postorbital; **pop**, postparietal; **pr?**, prootic?; **prf**, prefrontal; **sq**, squamosal. Scale bar equals 5 cm. [Intended for page width]

FIGURE 8. BP/1/5531, referred specimen of *Ufudocyclops mukanelai*, in **A**, dorsal, **B**, ventral, **C**, anterior, **D**, right lateral, **E**, left lateral, and **F**, occipital views. Scale bar equals 5 cm. [Intended for page width]

FIGURE 9. Phylogeny of Anomodontia, with position of *Ufudocyclops mukanelai* shown in bold. Numbers at nodes represent symmetric resampling values. [Intended for page width]

FIGURE 10. *Ufudocyclops* and *Angonisaurus* compared. **A**, **C**, holotype of *Ufudocyclops mukanelai* (BP/1/8208) in dorsal (**A**) and right lateral (**C**) views. **B**, **D**, holotype of *Angonisaurus cruickshanki* (NHMUK PV R9732) in dorsal (**B**) and left lateral (**D**; mirrored for comparative purposes) views. Scale bars equal 5 cm. [Intended for page width]

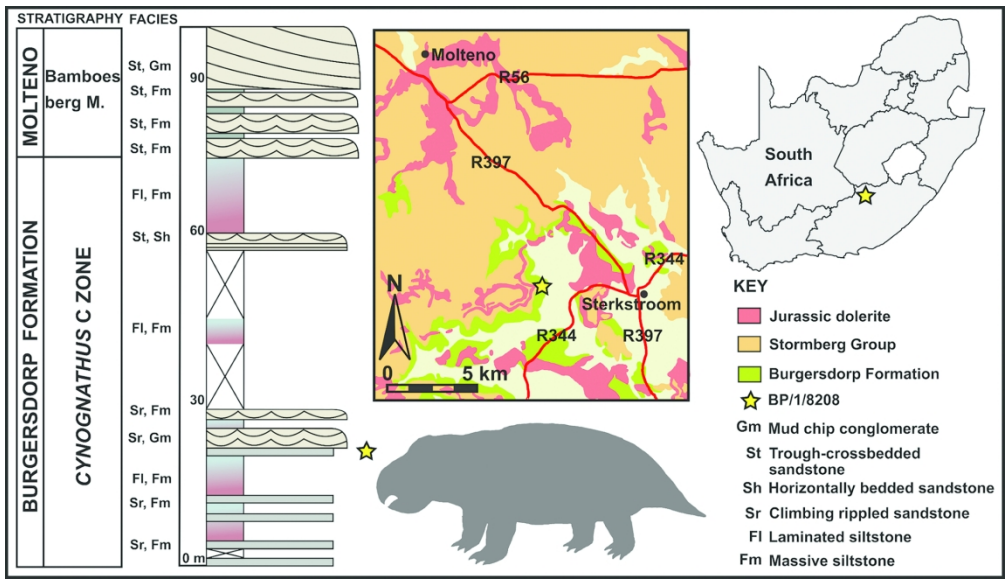

FIGURE 1. Geological context for BP/1/8208, holotype of Ufudocyclops mukanelai, showing position in stratigraphic section where specimen was discovered and site of the type locality. [Intended for page width]

183x104mm (300 x 300 DPI)

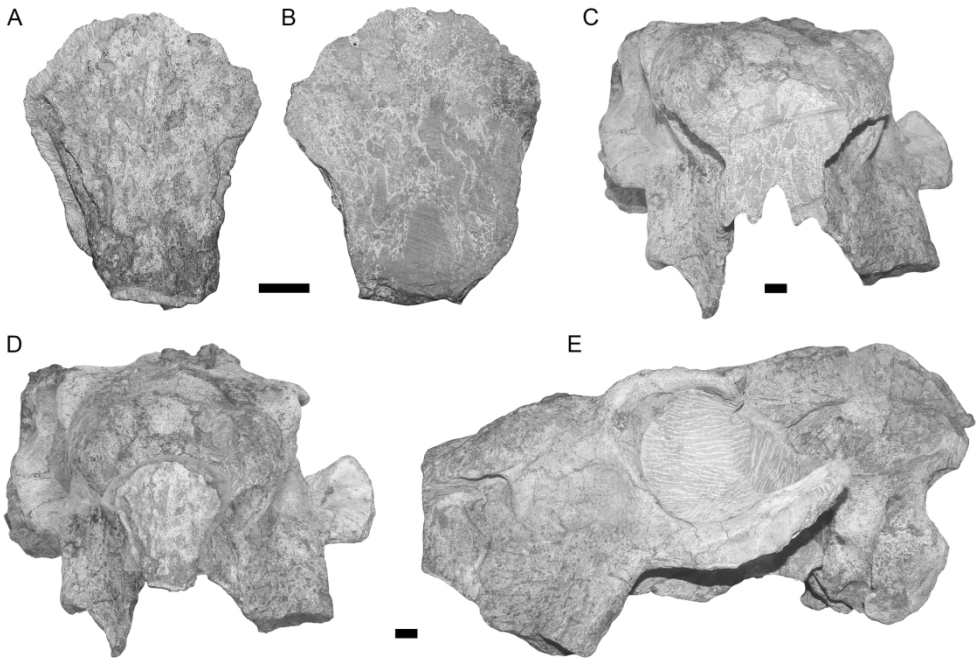

FIGURE 2. Photographs of BP/1/8208, holotype of Ufudocyclops mukanelai. Anterior fragment of premaxilla in A, anterior and B, posterior views. C, skull in anterior view with snout tip removed to show internal trabecular structure of premaxilla. D, skull in anterior view with snout tip in place. E, skull in left lateral view. Scale bars equal 1 cm. [Intended for page width]

182x125mm (300 x 300 DPI)

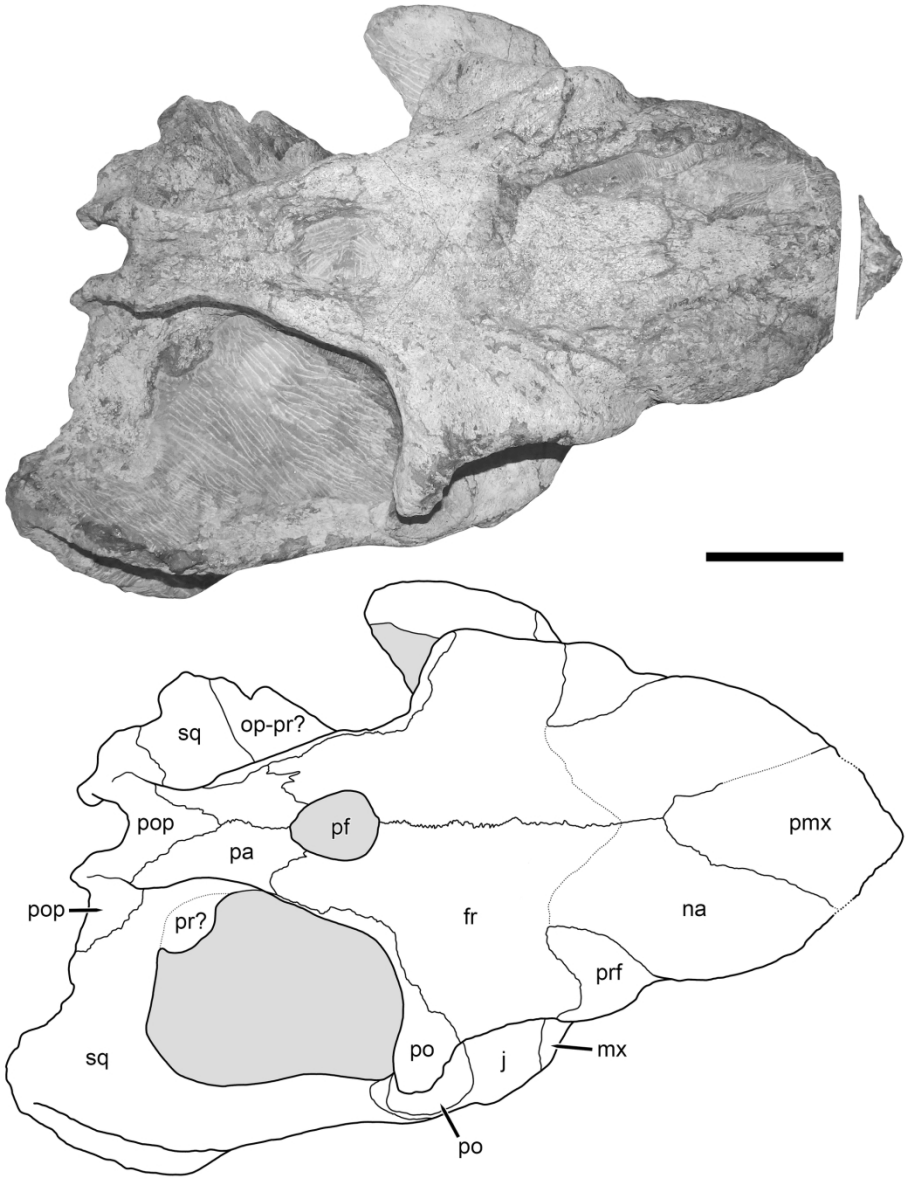

FIGURE 3. Photograph and interpretive drawing of BP/1/8208, holotype of Ufudocyclops mukanelai, in dorsal view. Abbreviations: fr, frontal; j, jugal; mx, maxilla; na, nasal; op, opisthotic; pa, parietal; pf, pineal foramen; pmx, premaxilla; po, postorbital; pop, postparietal; pr?, prootic; prf, prefrontal; sq, squamosal. Gray indicates matrix; dotted lines indicate uncertain sutural boundaries or missing bone. Scale bar equals 5 cm. [Intended for page width]

182x224mm (300 x 300 DPI)

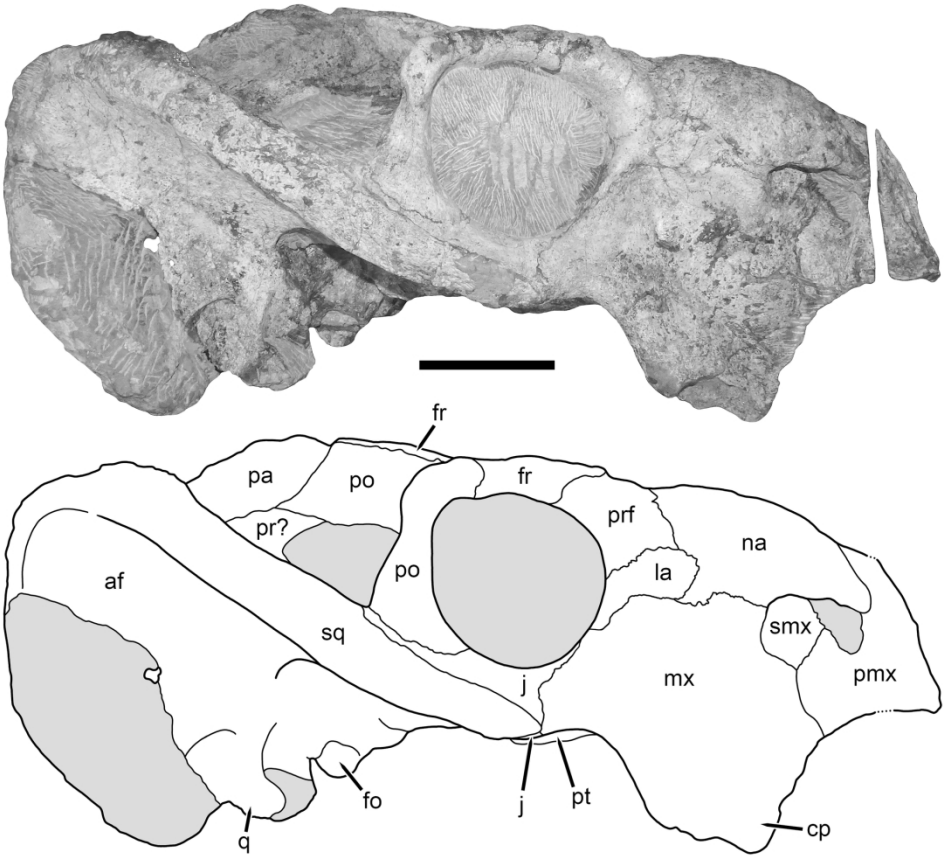

FIGURE 4. Photograph and interpretive drawing of BP/1/8208, holotype of Ufudocyclops mukanelai, in right lateral view. Abbreviations: af, fossa for M. adductor mandibulae externus lateralis; cp, caniniform process of maxilla; fo, fenestra ovalis; fr, frontal; j, jugal; la, lacrimal; mx, maxilla; na, nasal; pa, parietal; pmx, premaxilla; po, postorbital; pr?, prootic; prf, prefrontal; pt, pterygoid; q, quadrate; smx, septomaxilla; sq, squamosal. Gray indicates matrix; dotted lines indicate missing bone. Scale bar equals 5 cm. [Intended for page width]

182x160mm (300 x 300 DPI)

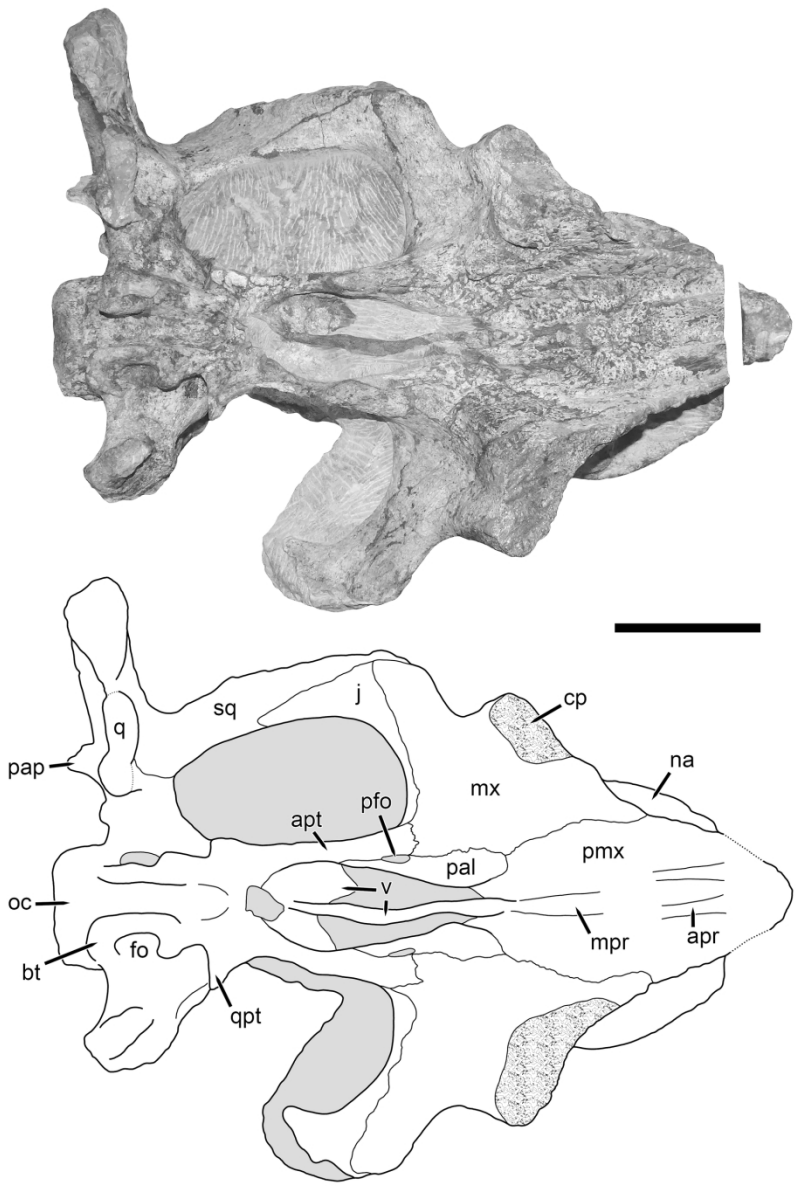

FIGURE 5. Photograph and interpretive drawing of BP/1/8208, holotype of Ufudocyclops mukanelai, in ventral view. Abbreviations: apr, anterior palatal ridge; apt, anterior pterygoid ramus; bt, basal tuber; fo, fenestra ovalis; j, jugal; mpr, median palatal ridge; mx, maxilla; na, nasal; oc, occipital condyle; pal, palatine; pfo, palatine foramen; pmx, premaxilla; pap, paroccipital process of opisthotic; q, quadrate; qpt, quadrate (=posterior) pterygoid ramus; sq, squamosal; v, vomer. Gray indicates matrix; patterning indicates broken edge of maxillary bone; dotted lines indicate uncertain sutural boundaries or missing bone. Scale bar equals 5 cm. [Intended for page width]

182x225mm (300 x 300 DPI)

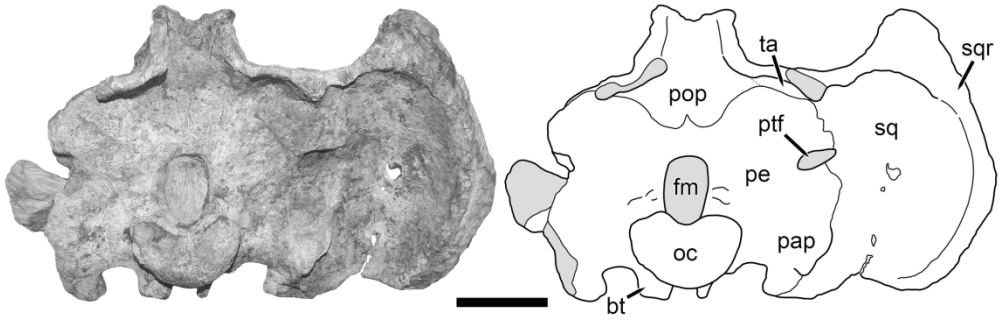

FIGURE 6. Photograph and interpretive drawing of BP/1/8208, holotype of Ufudocyclops mukanelai, in occipital view. Abbreviations: bt, basal tuber; fm, foramen magnum; oc, occipital condyle; pap, paroccipital process of opisthotic; pe, periotic; ptf, post-temporal fenestra; pop, postparietal; sq, squamosal; sqr, squamosal ridge; ta, tabular. Gray indicates matrix; dotted lines indicate uncertain sutural boundaries. Scale bar equals 5 cm. [Intended for page width]

182x61mm (300 x 300 DPI)

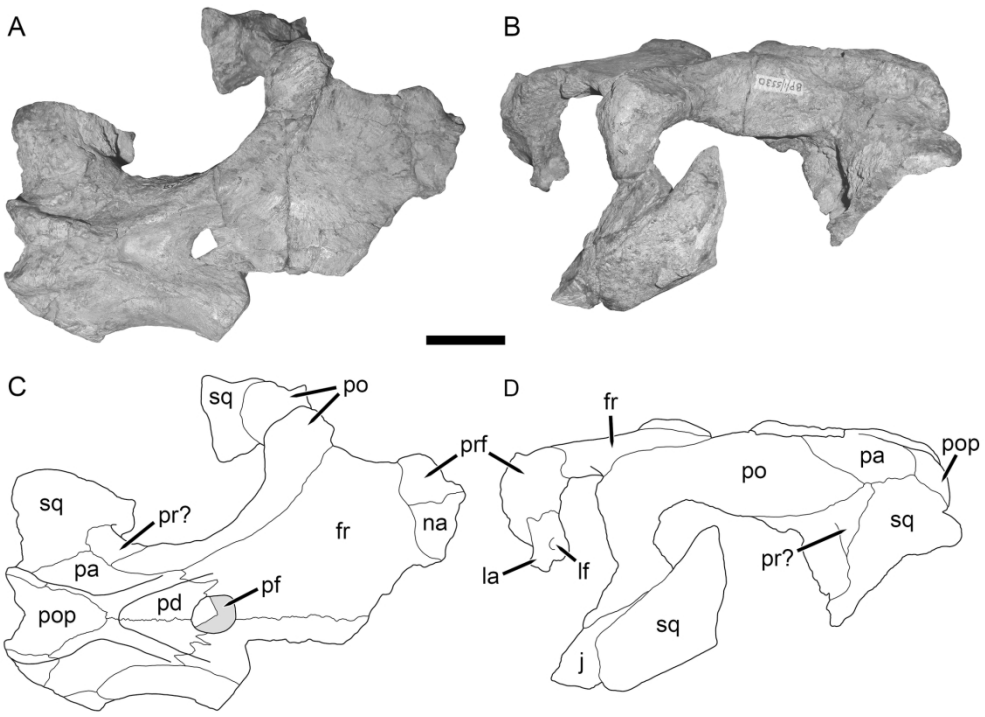

FIGURE 7. BP/1/5530, referred specimen of Ufudocyclops mukanelai, in A, dorsal (anterior is right) and B, left lateral views with C, D interpretive drawings. Abbreviations: fr, frontal; j, jugal; la, lacrimal; lf, lacrimal foramen; na, nasal; pa, parietal; pd, parietal depression; pf, pineal foramen; po, postorbital; pop, postparietal; pr?, prootic?; prf, prefrontal; sq, squamosal. Scale bar equals 5 cm. [Intended for page width]

182x135mm (300 x 300 DPI)

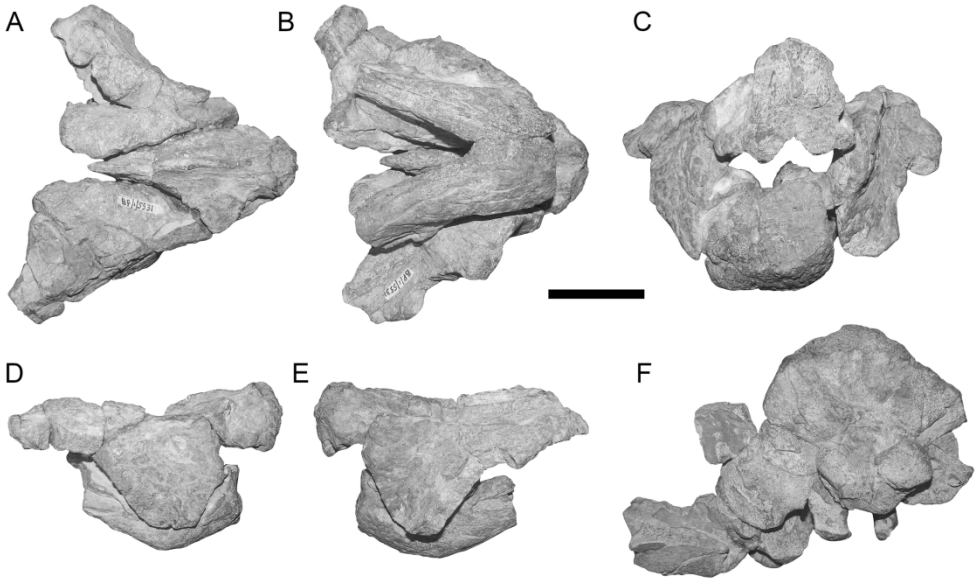

FIGURE 8. BP/1/5531, referred specimen of Ufudocyclops mukanelai, in A, dorsal, B, ventral, C, anterior, D, right lateral, E, left lateral, and F, occipital views. Scale bar equals 5 cm. [Intended for page width]

182x109mm (300 x 300 DPI)

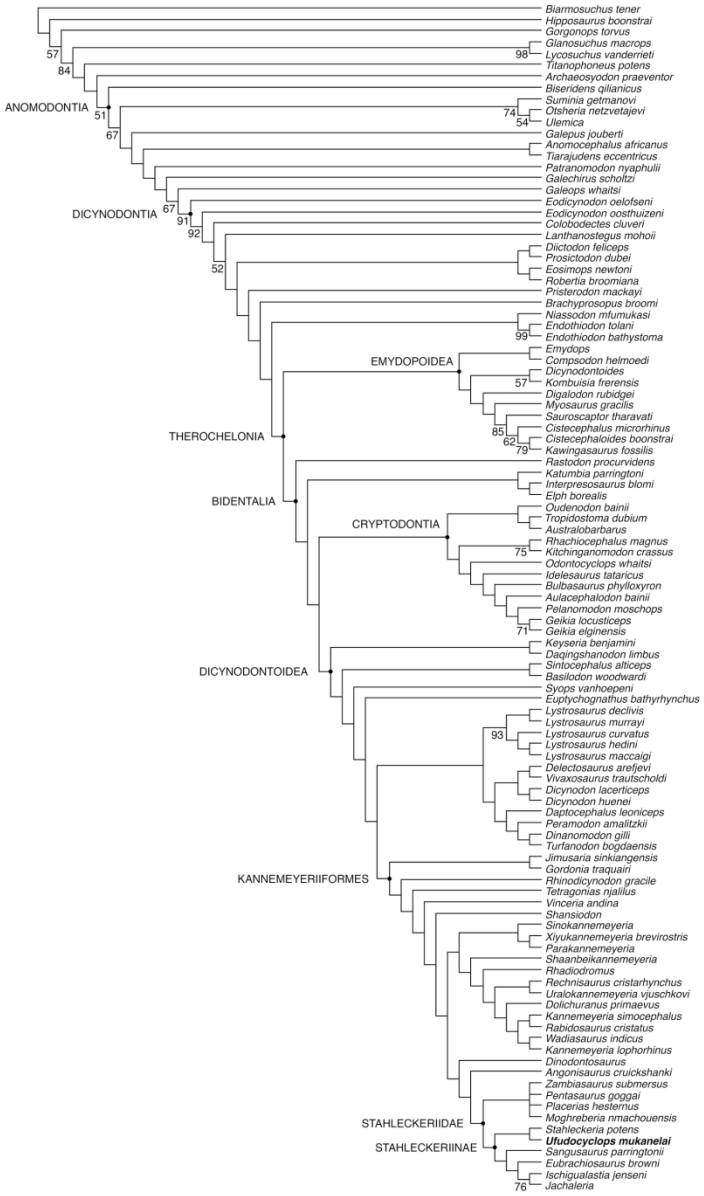

FIGURE 9. Phylogeny of Anomodontia, with position of Ufudocyclops mukanelai shown in bold. Numbers at nodes represent symmetric resampling values. [Intended for page width]

182x228mm (300 x 300 DPI)

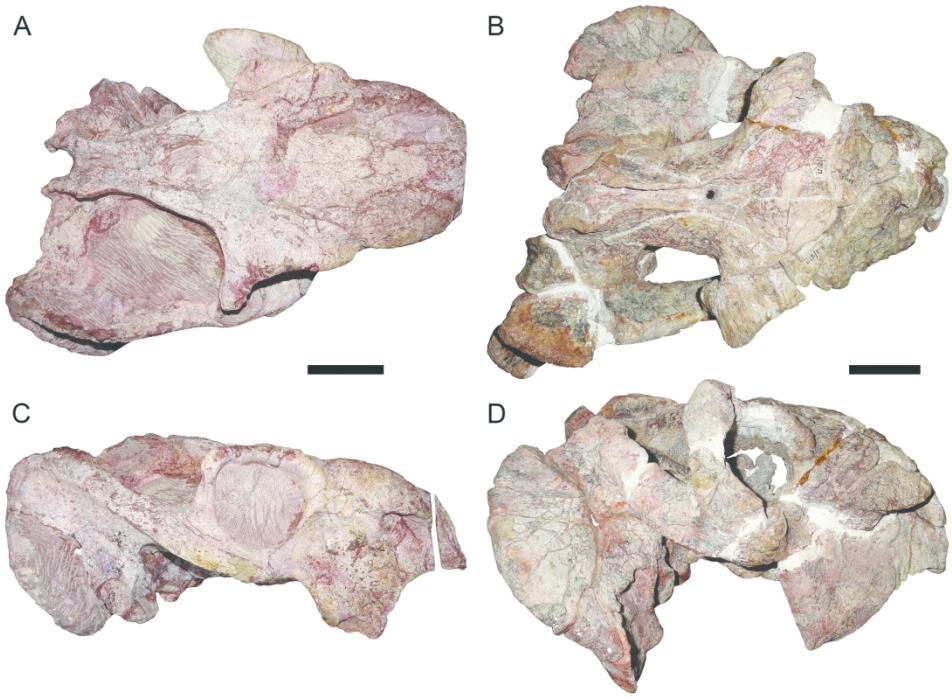

FIGURE 10. Ufudocyclops and Angonisaurus compared. A, C, holotype of Ufudocyclops mukanelai (BP/1/8208) in dorsal (A) and right lateral (C) views. B, D, holotype of Angonisaurus cruickshanki (NHMUK PV R9732) in dorsal (B) and left lateral (D; mirrored for comparative purposes) views. Scale bars equal 5 cm. [Intended for page width]

182x131mm (300 x 300 DPI)

TABLE 1. Cranial measurements of BP/1/8208, holotype of *Ufudocyclops mukanelai*, in centimeters. First four measurements are estimates based on gauge of saw to account for missing bone between anterior premaxillary tip and rest of snout.

Dorsal skull length	29.0
Basal skull length	29.5
Preorbital length	11.1
Pre-pineal skull length	19.0
Post-pineal skull length	6.9
Pineal foramen length	3.1
Pineal foramen width	2.9
Nasal boss length (right)	8.0
Nasal boss width (right)	4.3
Distance between nasal bosses	4.5
Interorbital width	13.8
Orbit length (right)	7.6
Orbit height (right)	7.1
Intertemporal bar anterior width	8.0
Intertemporal bar posterior width	3.6
Temporal fenestra length (right)	15.2
Secondary palate length	12.0
Anterior pterygoid keel height (right)	3.1
Anterior pterygoid ramus height (right)	2.2
Median pterygoid plate width	4.6